Sensitivity of Ring Analysis to Near-Surface Magnetism

Thierry Corbard

Observatoire de la Côte d'Azur

Nice, France

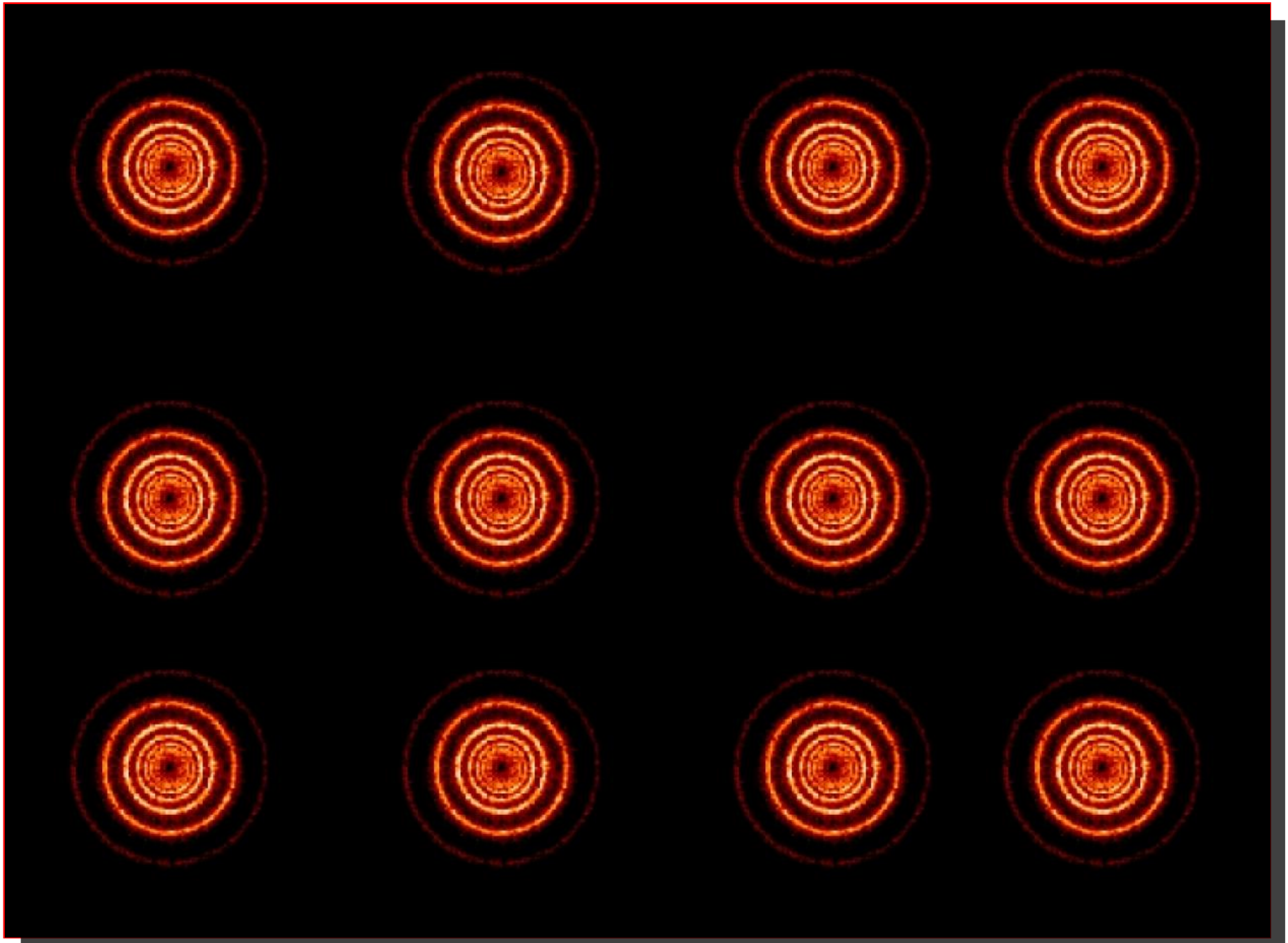

Motivation for ring diagrams: Global Helioseismology limitations

- Sensitive only to the part of the rotation that is symmetric about the equator.
- Kernels Independent of longitude (e.g. cannot infer interaction between an active region and sub-surface flows)
- Impossible to separate the spherically asymmetric effects other than rotation (meridional circulation, magnetic fields, structural asphericity)
- Difficulty of fitting high-ℓ modes in global analysis due to mode leakage

Ring Diagram Analysis Principles

- Général Dispersion Relationship for global modes:

$$k_r^2 + k_h^2(1 - N^2/\omega^2) = (\omega^2 - \omega_c^2)/c^2 \qquad K_h^2 = \ell(\ell+1)/r^2 = K_\theta^2 + K_\varphi^2$$

- Because the wavelength of high order modes is small compared with the typical scale over which equilibrium structure changes, the modes can be approximated locally by plane sound waves

$$\Rightarrow \quad k^2 = k_z^2 + k_h^2 = \omega^2/c^2 \qquad K_h^2 = K_x^2 + K_y^2$$

- High degree (ℓ >300) acoustic waves are damped and cannot travel around the full circumference of the sun. Their horizontal wave number isn't quantized anymore and their frequencies are local measures of the sun's properties.

Ring Diagram Analysis Principles

The presence of a velocity field, $\boldsymbol{U}$, will perturb the frequency by advecting the wave front and producing an apparent Doppler shift $\Delta\omega$, given by

$$\Delta\omega = \boldsymbol{k} \cdot \boldsymbol{U} = k_x U_x + k_y U_y \,, \qquad (2)$$

where U_x and U_y are the x and y components of the velocity vector $\boldsymbol{U}$. More precisely, $\boldsymbol{U}$ is an average over depth of the velocity with a weighting given by an average of the kernels of the modes contained in the ring.

Hill, 1988

=> $\omega = \omega_0 + \Delta\omega = c\,k + k_x\,U_x + k_y\,U_y$

Ring Diagram Analysis Principles

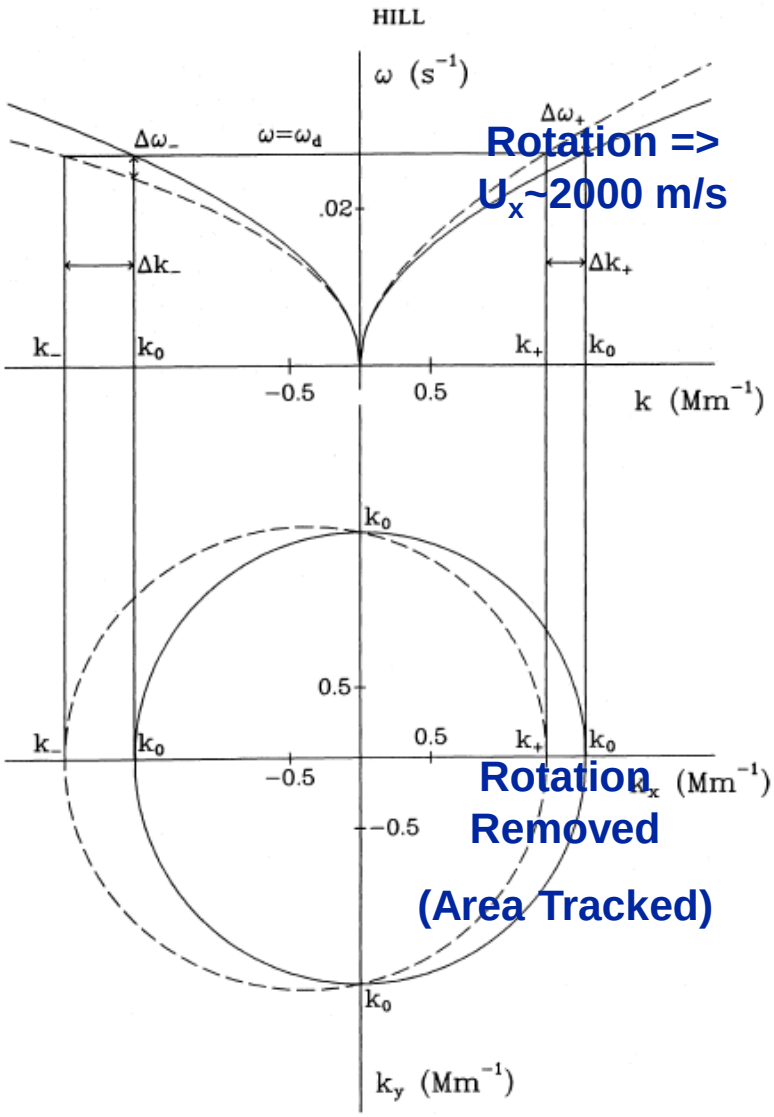

Rotation => U_x~2000 m/s

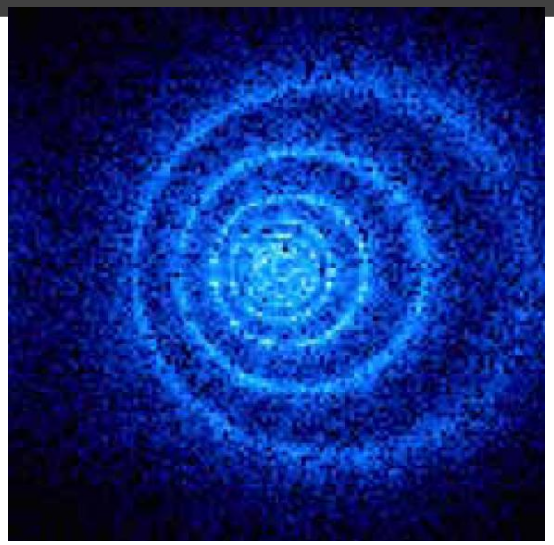

Rotation Removed

(Area Tracked)

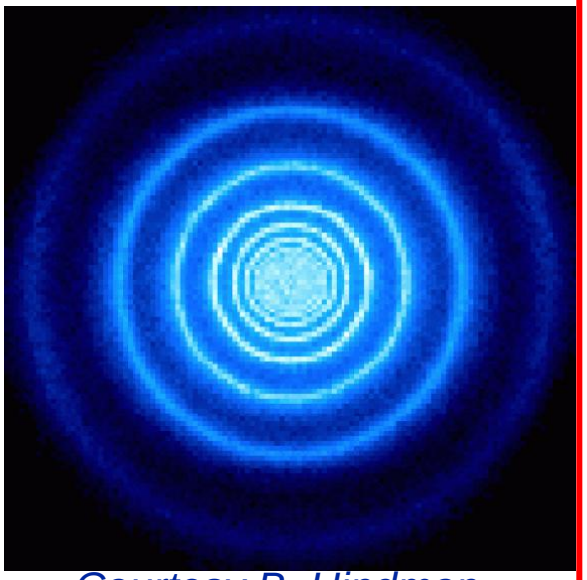

Courtesy B. Hindman

Step 1 : Tracking

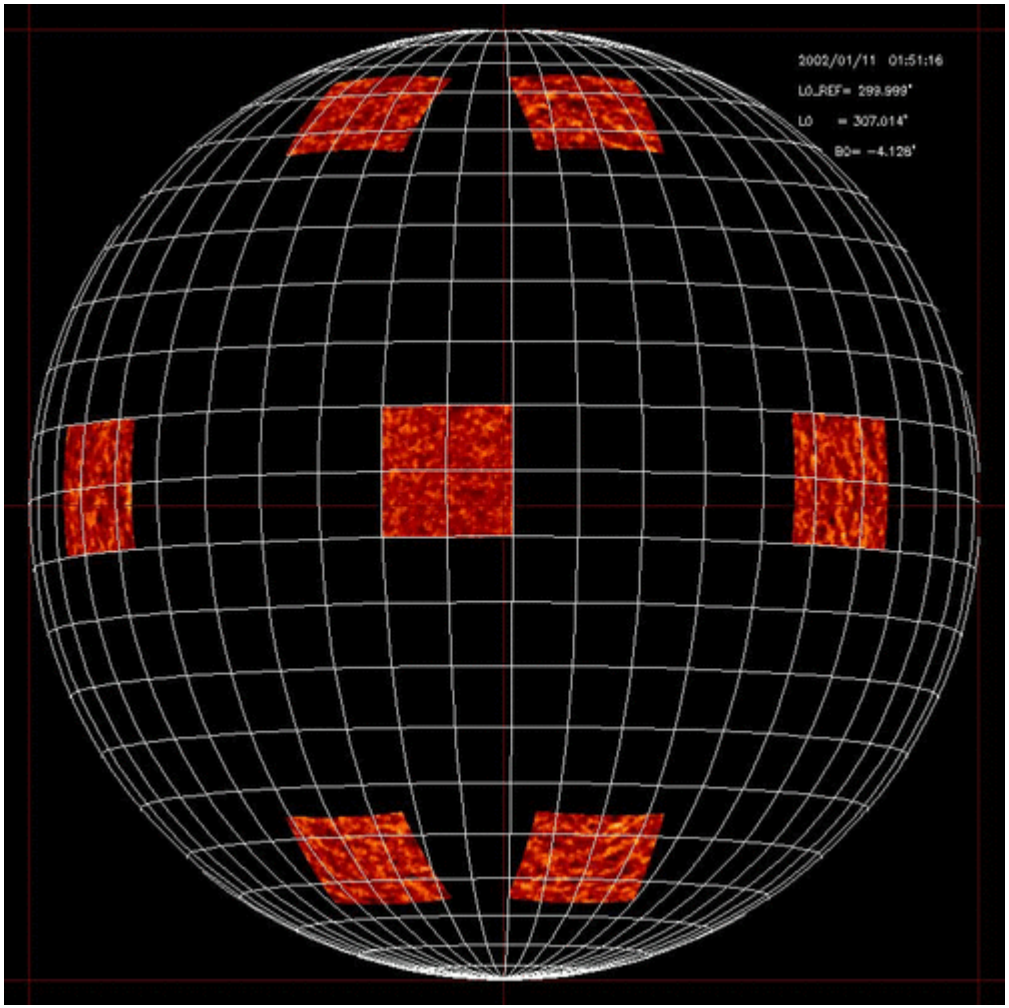

- Small areas (16ºx16º) are tracked (typically 1664 mn) over the solar disk at a rate depending on the latitude of their center.
- These areas are remapped using a Postel or transverse cylindrical projection that tend to preserve the distance along great circles.
- => Data cubes (Latitude – Longitude – time)

Steps 2-3-4

3D FFT → **3D Power spectra Fitting**

$(\theta,\varphi,t) \rightarrow (k_x,k_y,\omega)$

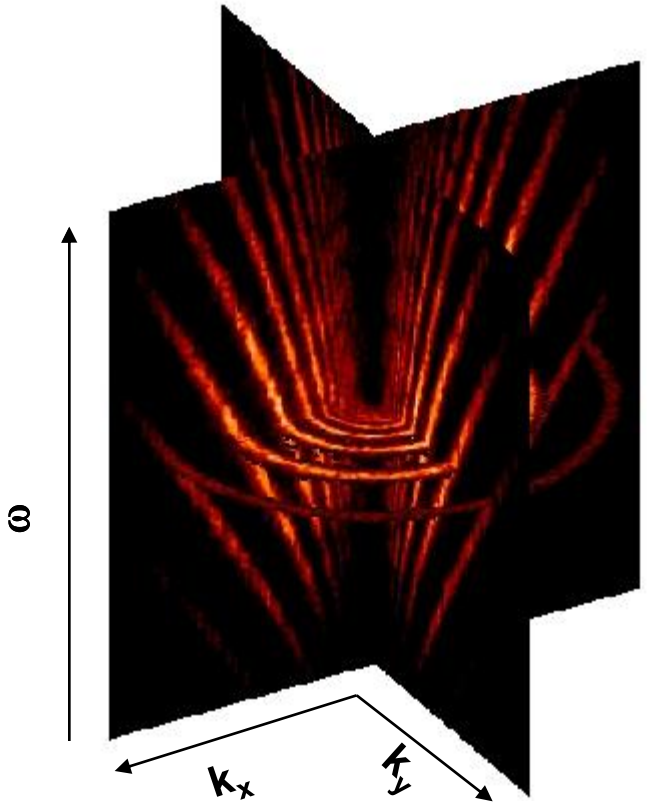

$$P = \frac{A\,\Gamma}{(\omega - \omega_0 + k_x U_x + k_y U_y)^2 + \Gamma^2} + \frac{b_0}{k^3}$$

16 deg patch, 1664mn @ 1mn cadence

- Nyquist frequency 8.33mHz
- Nyquist wavenumber ~ ℓ=1440
- $\Delta\nu \sim 10\mu$Hz
- Δk ~> 22 ℓ values per wavenumber bin

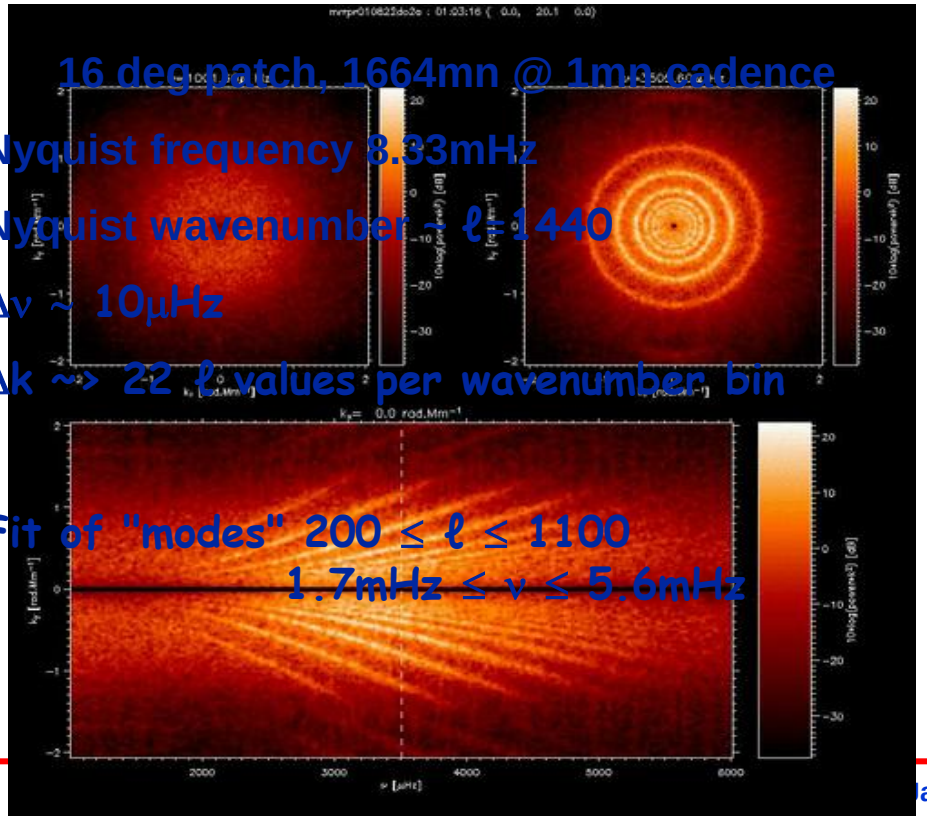

- Fit of "modes" $200 \le \ell \le 1100$
  $1.7\text{mHz} \le \nu \le 5.6\text{mHz}$

Effect of Magnetic Field on high degree modes sensed by rings

Effect of Magnetic Field on high degree modes sensed by rings: what to expect?

- Sunspot scatter and absorb p-modes.
- Amplitude of solar oscillations decrease significantly in active regions.
  - Absorption of acoustic modes / weaker excitation in active regions
- There are well known temporal variations of global modes mean frequencies, amplitude, linewidth…with the cycle
  - If one believes this is the effect of global magnetic field variation then one should expect a much larger effect if modes in active region are studied separately (B_{AR}>> max(<B>))
- High degree modes: very short horizontal wavelengths and short lifetimes (<<sound travel time around the Sun)
  - Local effects are expected to be more important for these modes
  - This may compensate for larger statistical error (smaller spatial and temporal intervals covered)

Fractional amplitude (total power) changes

Howe et al. 2004

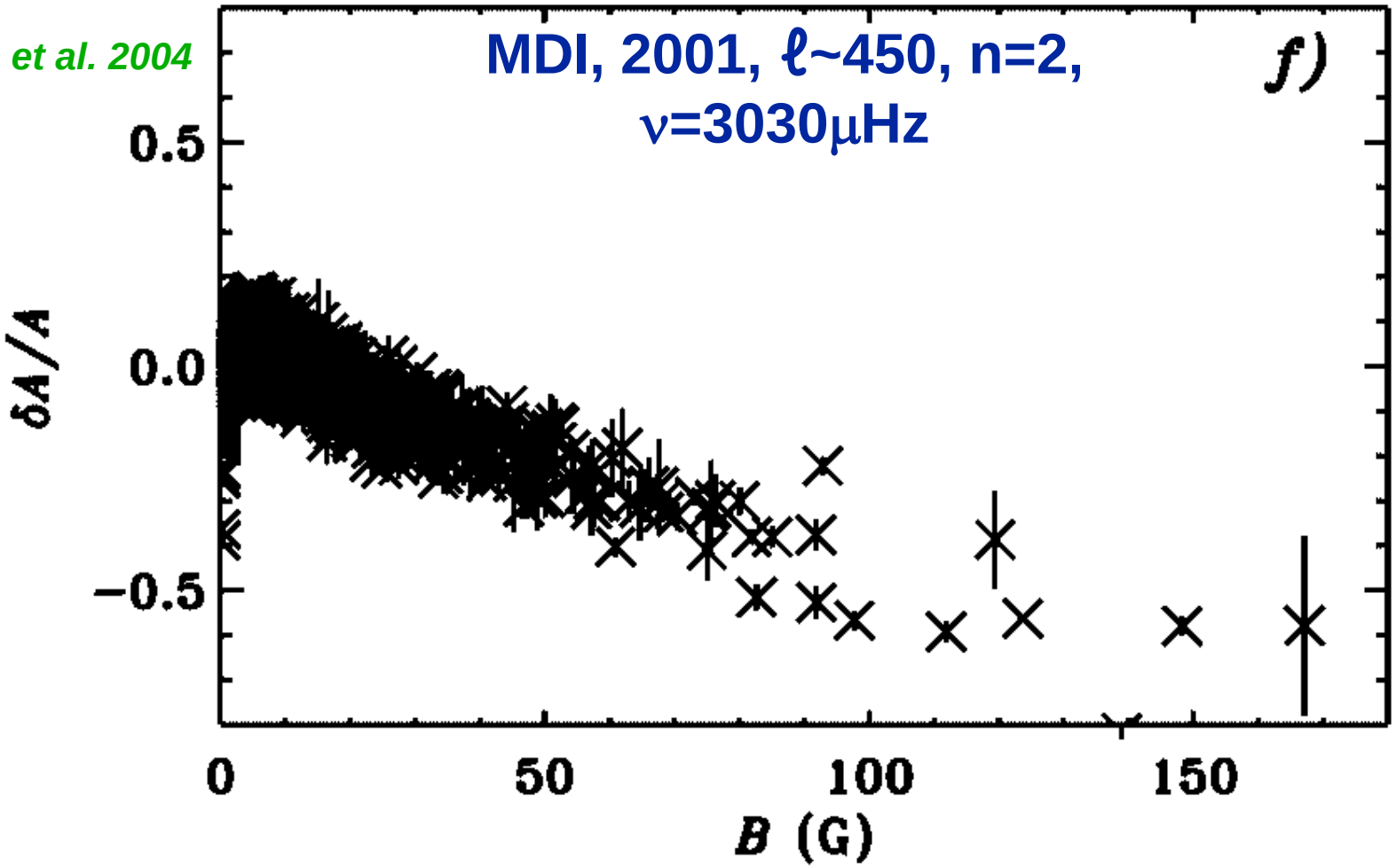

Mode power clearly reduced in active regions

Fractional amplitude (total power) changes

Howe et al. 2004

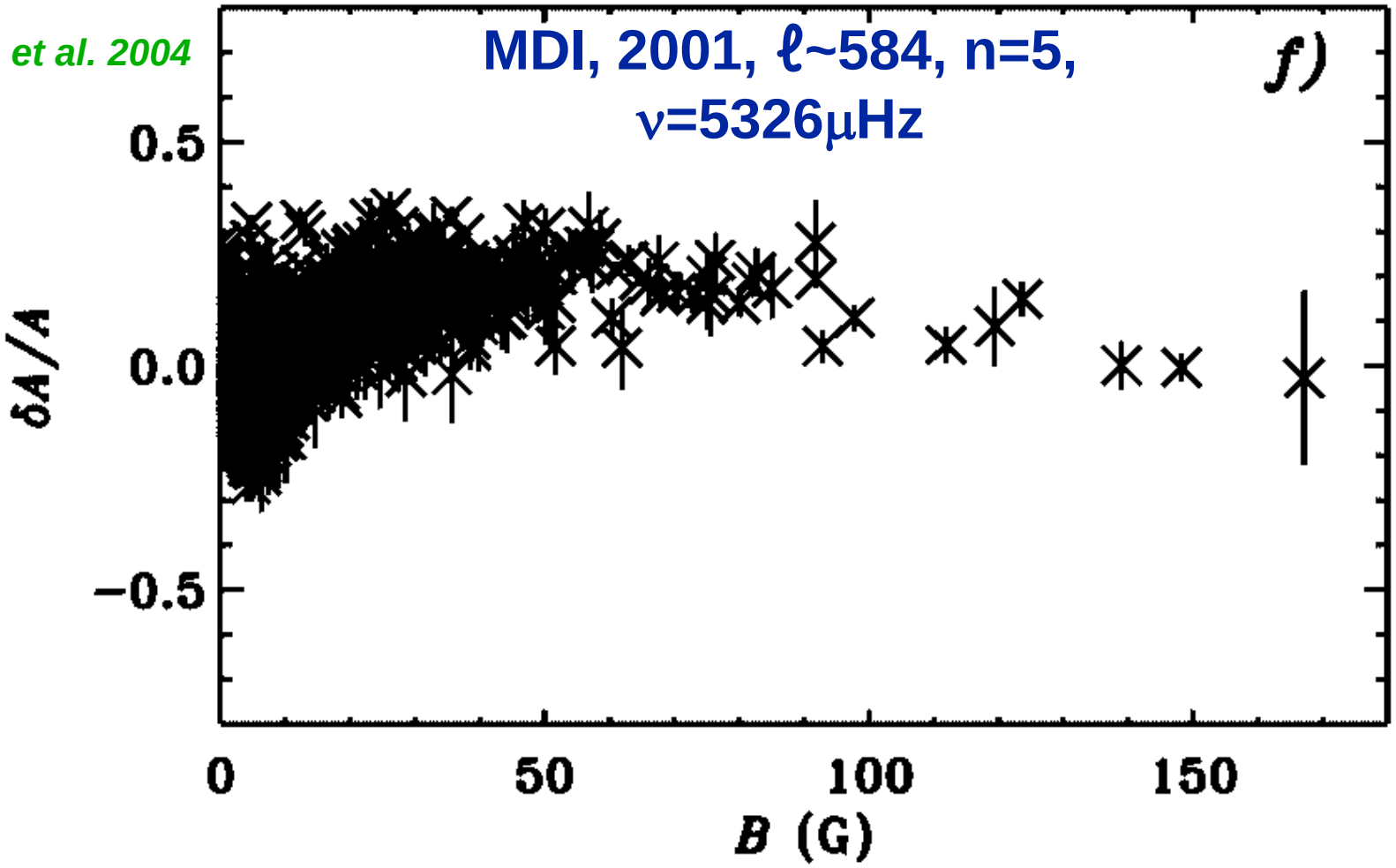

Amplitudes enhanced in active regions except for the highest activity levels

Fractional amplitude (total power) changes

Howe et al. 2004

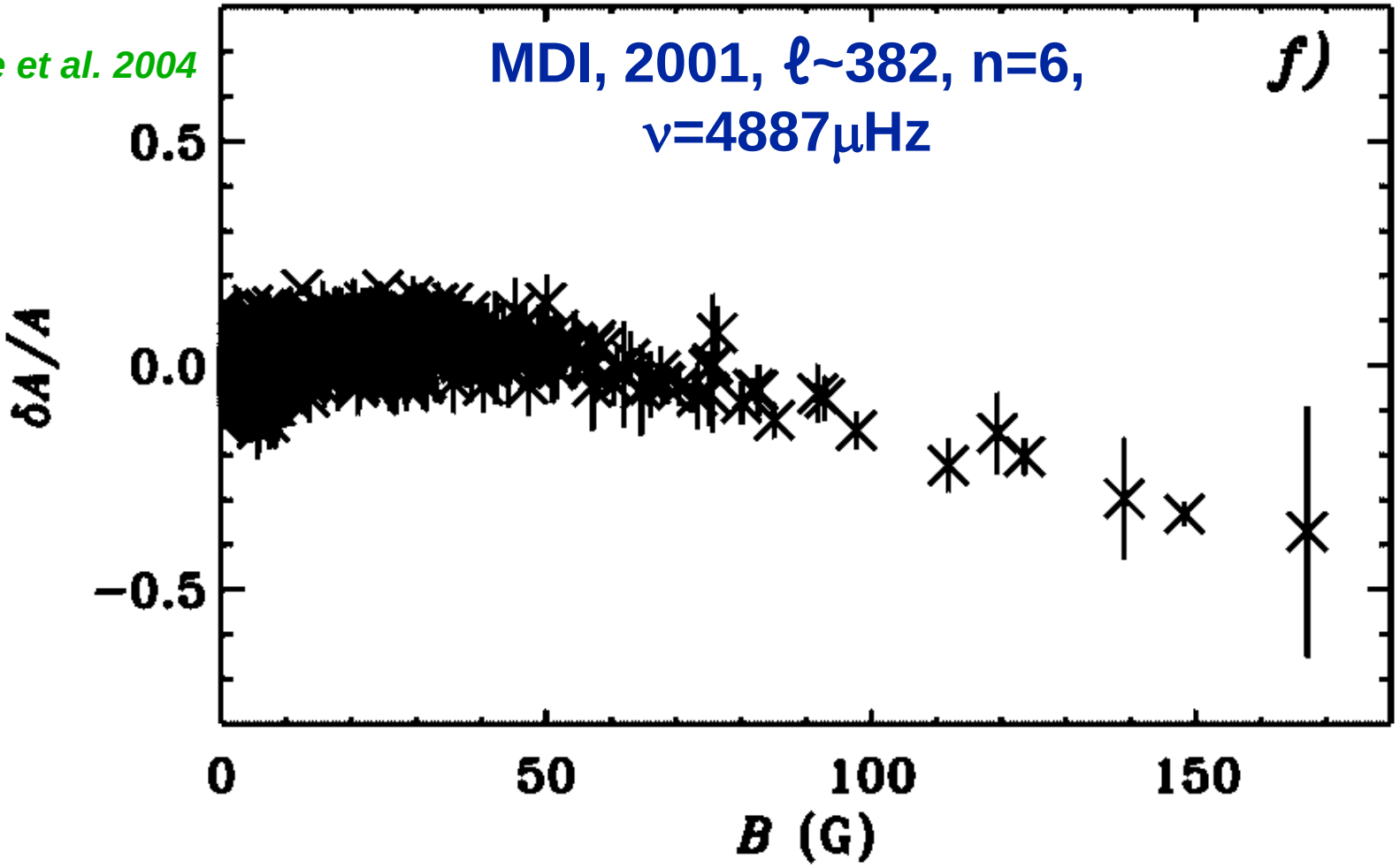

Like p-modes (supressed in active regions) at high B
Like high-frequency waves (enhanced in actives regions) at lower activity levels

Fractional amplitude (total power) changes

Howe et al. 2004

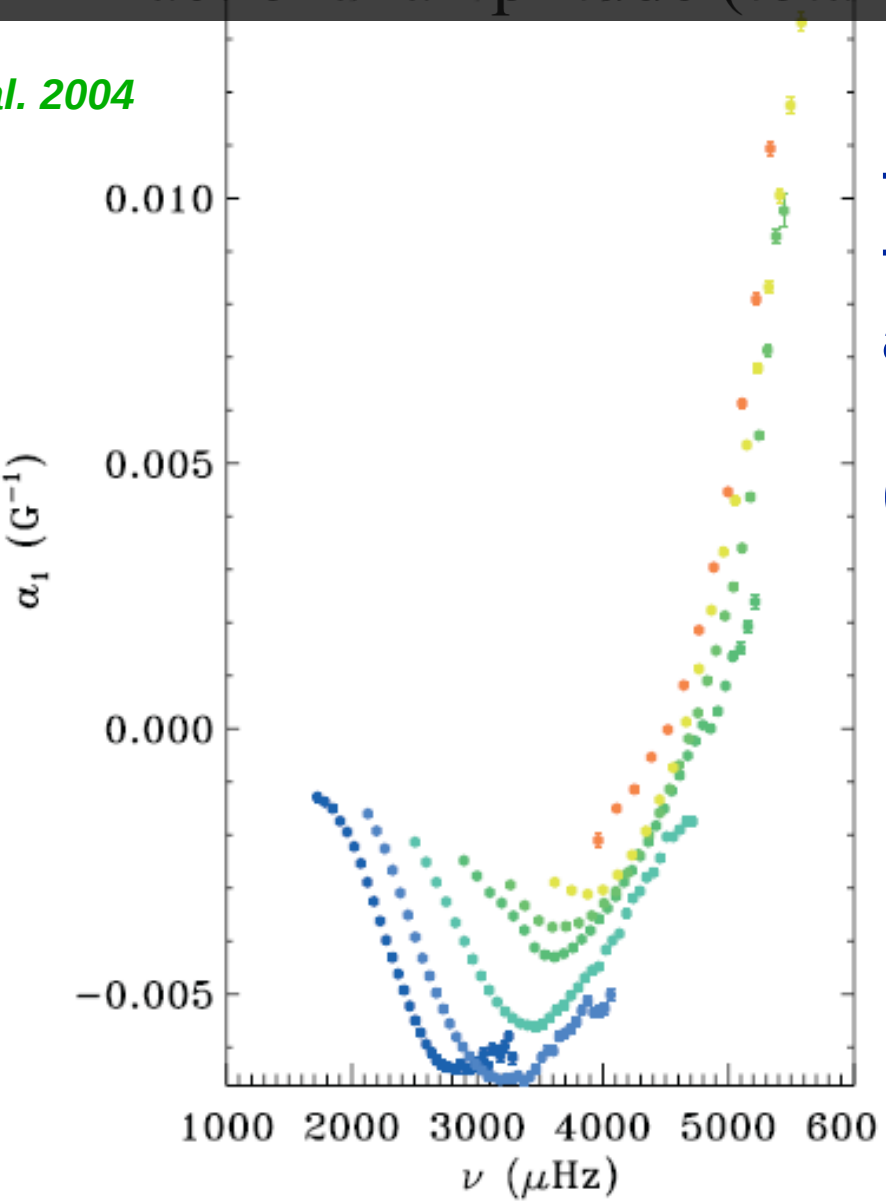

First order coefficient for quadratic fit to fractional peak amplitude changes vs. magnetic flux (MDI 1996-2002, n=0-6)

Fit with asymmetric peak profile *Rajaguru, Basu & Antia 2001*

$$P(k_x, k_y, \nu) = \left\{ \exp\left[A_0 + (k - k_0)A_1 + A_2\left(\frac{k_x}{k}\right)^2 + A_3 \frac{k_x k_y}{k^2} \right] \times [S^2 + (1 + Sx)^2] \right\} (x^2 + 1)^{-1} + \frac{e^{B_1}}{k^3} + \frac{e^{B_2}}{k^4}, \quad (1)$$

where

$$x = \frac{\nu - ck^p - U_x k_x - U_y k_y}{w_0 + w_1(k - k_0)}, \quad (2)$$

$k^2 = k_x^2 + k_y^2$, k being the total wavenumber, and the 13 parameters A_0, A_1, A_2, A_3, c, p, U_x, U_y, w_0, w_1, S, B_1, and B_2 are determined by fitting the spectra using a maximum likelihood approach (Anderson, Duvall, & Jefferies 1990).

Compare the mode characteristics of 18 pairs of regions from MDI data (1996-2000)

(quiet/active at the same latitude and Carrington rotation and crossing central meridian)

=> Avoid foreshortening, distortion and varying focus/plate scale effects

Mean frequency shifts with activity level

Rajaguru, Basu & Antia 2001

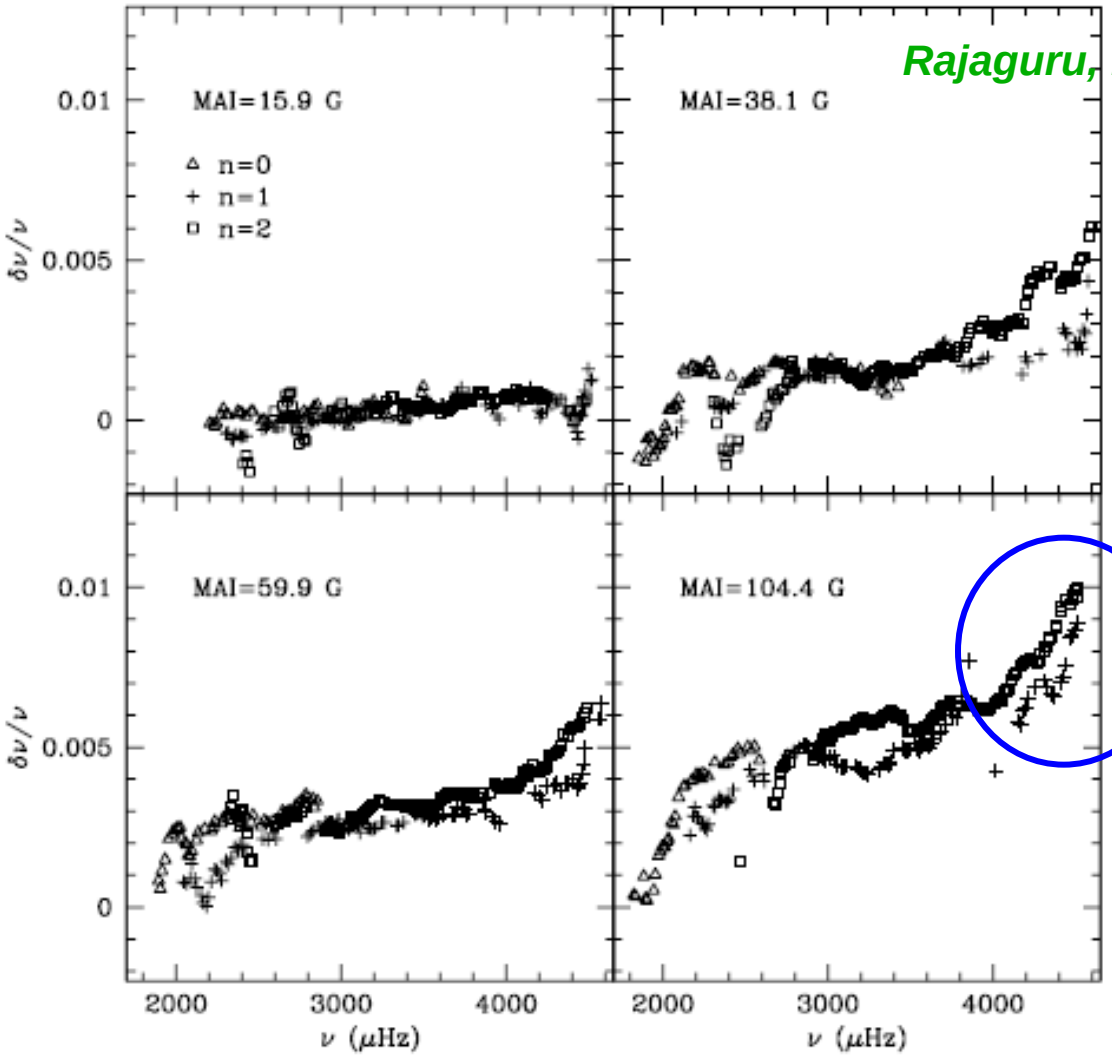

FIG. 1.—Relative frequency differences as a function of frequency for four different pairs of regions. The error on the points is about 0.0004 at 3.5 mHz and increases to 0.0007 above 4.5 mHz. The MAI for the active region in each pair is indicated in the panels.

No decrease seen in frequency shifts between 4 and 4.6mHz

Mean frequency shifts with activity level

Rajaguru, Basu & Antia 2001

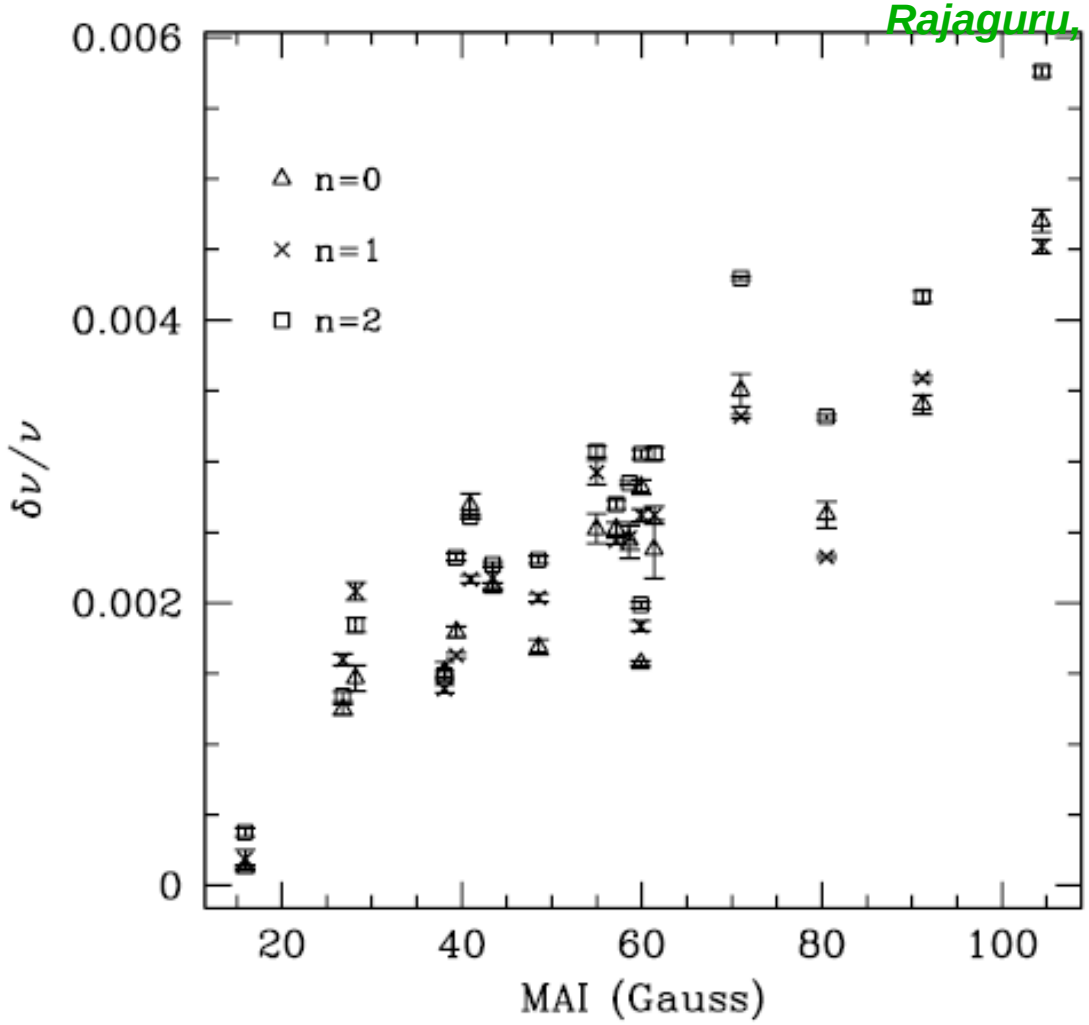

FIG. 2.—Average relative frequency differences plotted as a function of the magnetic activity index. Frequency differences of *f*-modes have been averaged over modes in the frequency range 2550–2750 μHz, while those of *p*-modes have been averaged over modes in the range 3000–3500 μHz. The averaging over the relatively narrow frequency range is necessary because of the steep frequency dependence of $\delta\nu/\nu$.

Linewidths

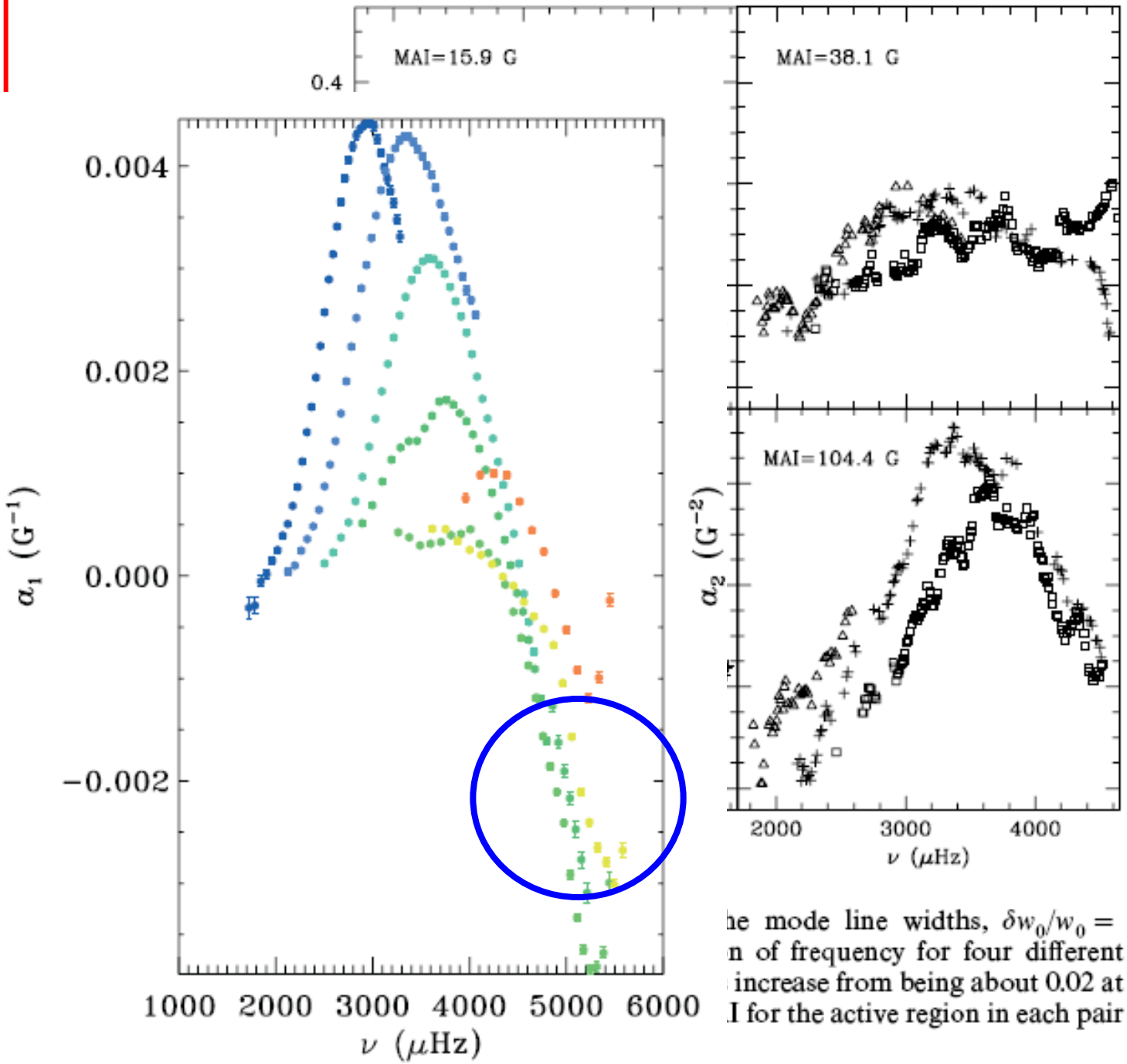

he mode line widths, $\delta w_0/w_0 =$
n of frequency for four different
increase from being about 0.02 at
I for the active region in each pair

High frequency waves lifetimes are enhanced for medium MAI

Tripathy et al. 2008

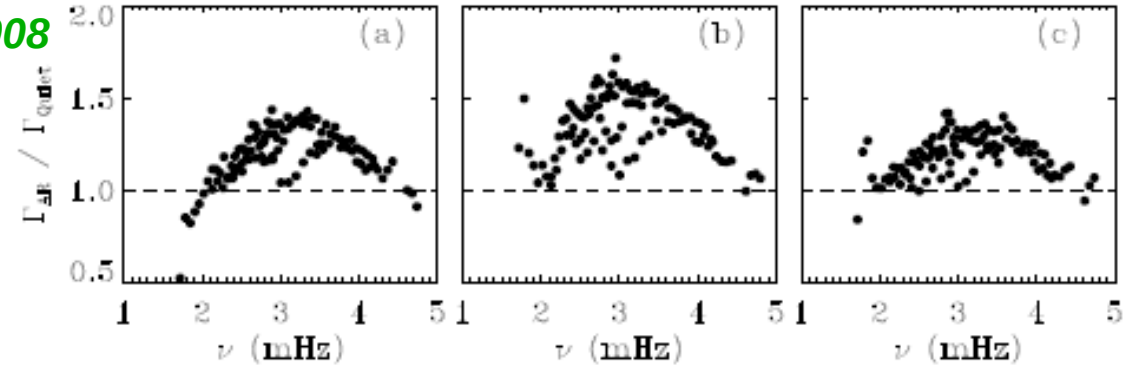

Active Region

Figure 4. Same as Figure 2 but for the active region NOAA 9628.

Oscillation modes in the source location of CMEs with a low value of magnetic flux have higher life time as compared to the quiet regions

=> Damping process slower than in quiet regions
=> may be used to forecast AR which may trigger CMEs

Effect of Magnetic Field on subsurface flows sensed by rings

Inverting for the flows

3D FFT → **3D Power spectra Fitting**

$(\theta, \varphi, t) \rightarrow (k_x, k_y, \omega)$

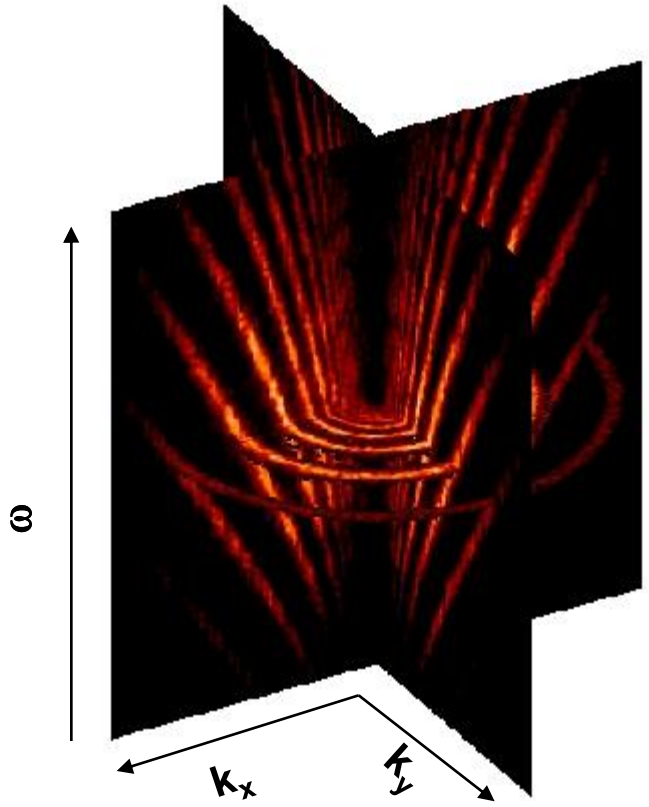

$$P = \frac{A\,\Gamma}{(\omega - \omega_0 + k_x U_x + k_y U_y)^2 + \Gamma^2} + \frac{b_0}{k^3}$$

2 x 1D Inversions

$$U_{x,y}(\omega_o, k_h) = \int K(\omega_o, k_h, z) v_{x,y}(z) dz$$

V_z may then be computed using the divergence of the horizontal flow and assuming mass conservation.

(Komm, Corbard et al. 2004)

Sensitivity of the wavefield to weak local flows using Born approximation

$$u_j^{(kn)} = \sum_{s=x,y,z} \int\int\int_{\odot} d\boldsymbol{r}\, K_{js}^{(kn)}(\boldsymbol{r}) v_s(\boldsymbol{r}).$$

K_{xx} **K_{xy}** **K_{xz}**

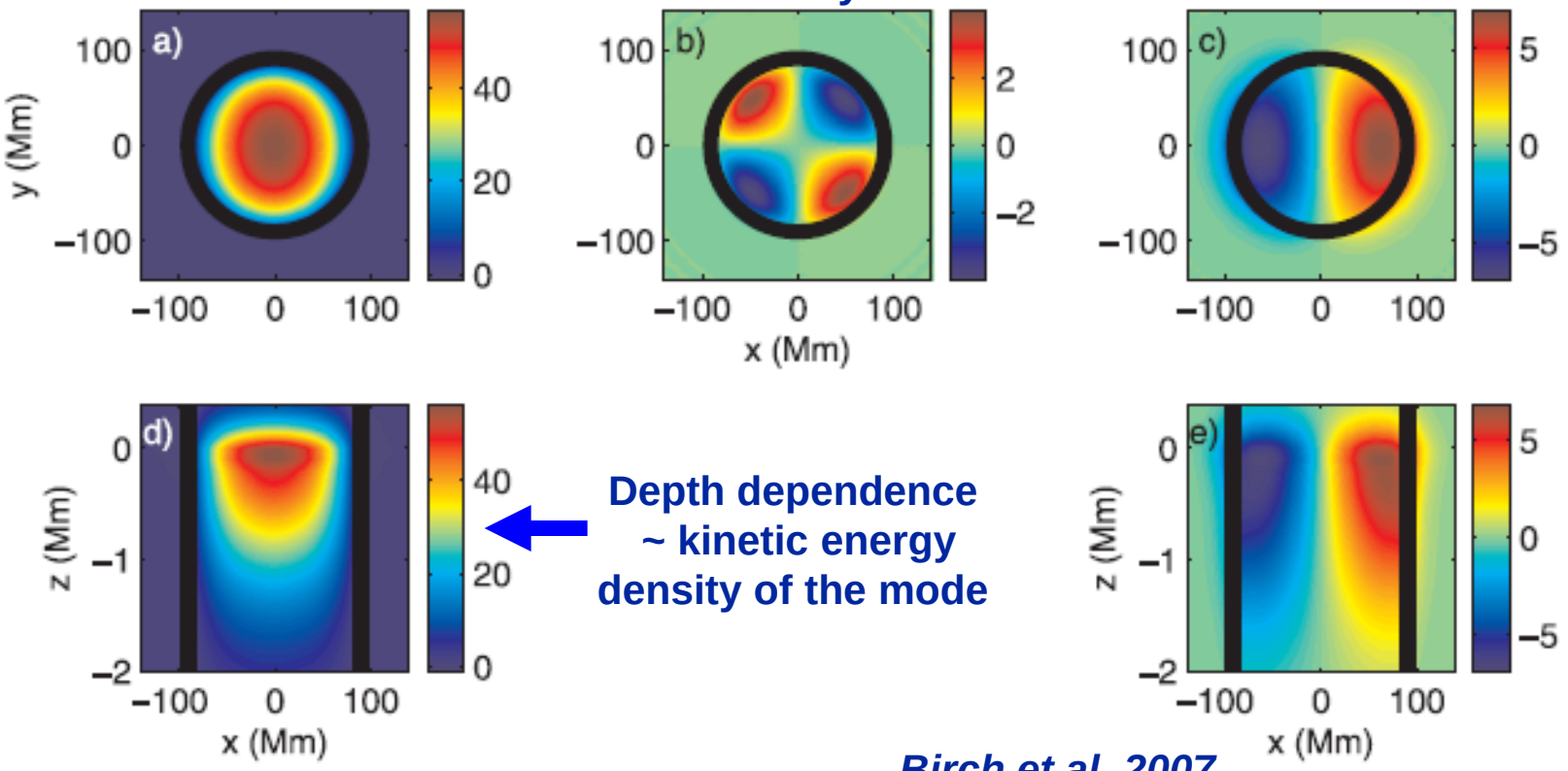

Depth dependence ~ kinetic energy density of the mode

Birch et al. 2007

Computing Vz using the continuity equation

Using the continuity equation (representing mass conservation), we estimate the vertical velocity component from the measured divergence of the horizontal flow (Scorer 1978; Holton 1979). The continuity equation can be written as follows

$$\frac{\partial \rho}{\partial t} + \nabla\rho \cdot \vec{v} + \rho \cdot \nabla\vec{v} = 0 \tag{3}$$

where ρ is the density and $\vec{v}$ is the 3-dimensional velocity vector. Since each data point represents an average over 1664 minutes, we neglect the term of the temporal density fluctuations. In addition, we assume that any horizontal density variations average out over the area of a dense-pack patch. The density is simply a function of radius. The continuity equation can then be simplified to

$$\frac{\partial v_z}{\partial z} + \left(\frac{1}{\rho}\frac{\partial \rho}{\partial z}\right) v_z + \operatorname{div} v = 0 \tag{4}$$

where $\operatorname{div} v$ is the horizontal flow divergence (Equation 1). This equation has the following solution:

$$v_z(d) = -\frac{1}{\rho}\int_{R_\odot}^{R_\odot - d} \rho \operatorname{div} v \, \mathrm{d}z + v_\odot \frac{\rho_\odot}{\rho} \tag{5}$$

Synoptic Flow Maps

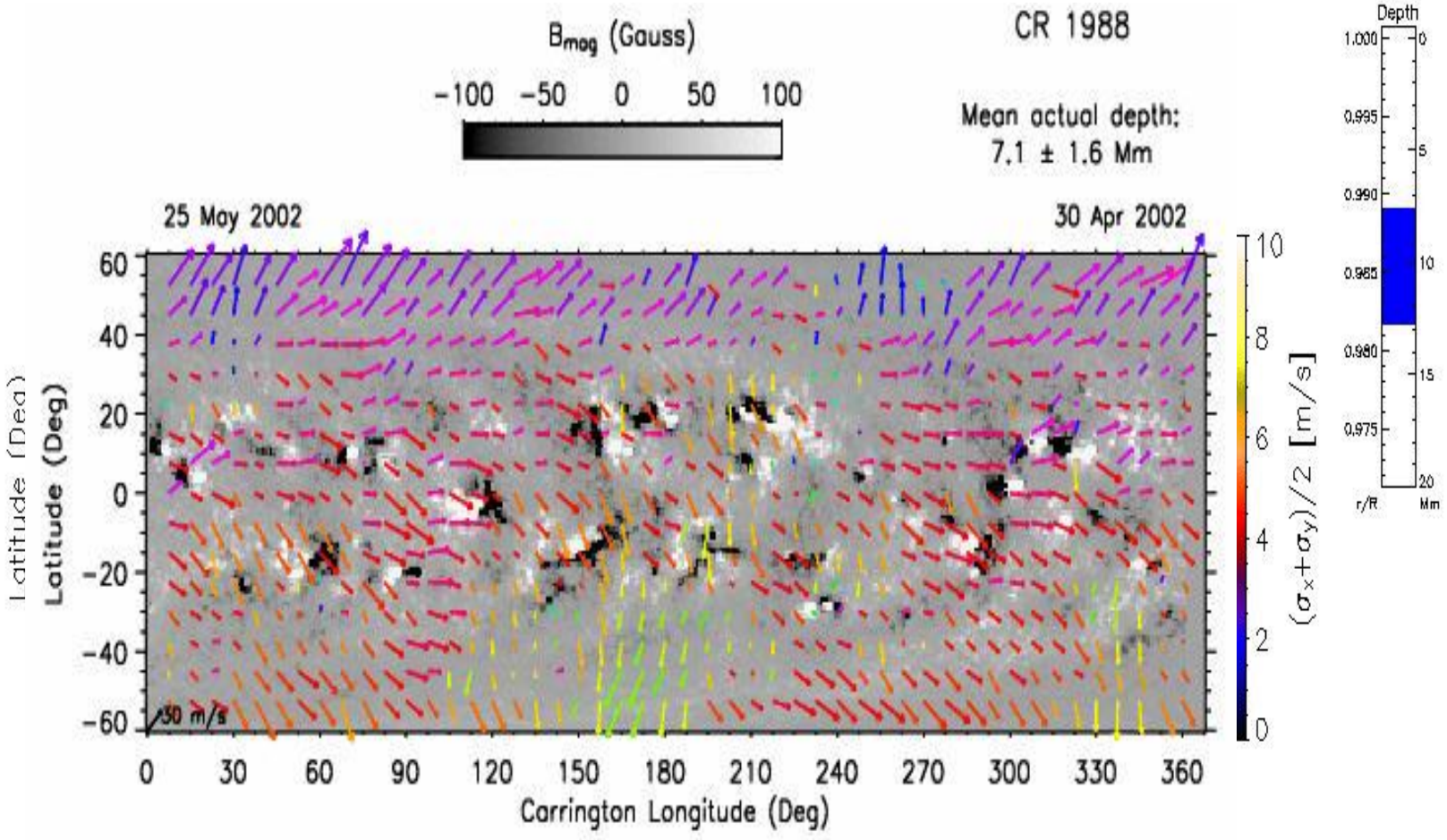

Some fluid descriptors

From the daily flow maps, we calculate the divergence of the horizontal flow components and the vertical vorticity component

$$\operatorname{div} v = \frac{\partial v_x}{\partial x} + \frac{\partial v_y}{\partial y} \tag{1}$$

$$\operatorname{vort} v = \frac{\partial v_y}{\partial x} - \frac{\partial v_x}{\partial y} \tag{2}$$

where v_x is the zonal and v_y is the meridional flow component. We use $\operatorname{div} v$ and $\operatorname{vort} v$ to distinguish the components from the complete divergence $(\nabla \vec{v})$ and vorticity $(\nabla \times \vec{v})$. We then calculate synoptic maps of these quantities in the same way as for the velocities. In addition, we calculate the vertical gradients, $\partial v_x/\partial z$ and $\partial v_y/\partial z$, of the horizontal flow components and the corresponding synoptic maps. All quantities are functions of latitude, longitude, and depth.

Kinetic Helicity

The kinetic helicity of a fluid flow is the integrated scalar product of the velocity field, $\vec{v}$, and the vorticity field, $\nabla \times \vec{v}$ (Moffatt & Tsinober 1992):

$$\mathcal{H} = \int \vec{v} \cdot \nabla \times \vec{v} \; dV \tag{7}$$

where $\vec{v} \cdot \nabla \times \vec{v}$ is called the helicity density of the flow. The kinetic helicity and its density are pseudoscalar quantities. If the vorticity is a stationary random quantity (for example, homogeneous turbulence), one can define the mean helicity

$$H = \langle \vec{v} \cdot \nabla \times \vec{v} \rangle \tag{8}$$

Divergence of horizontal flow (div v)

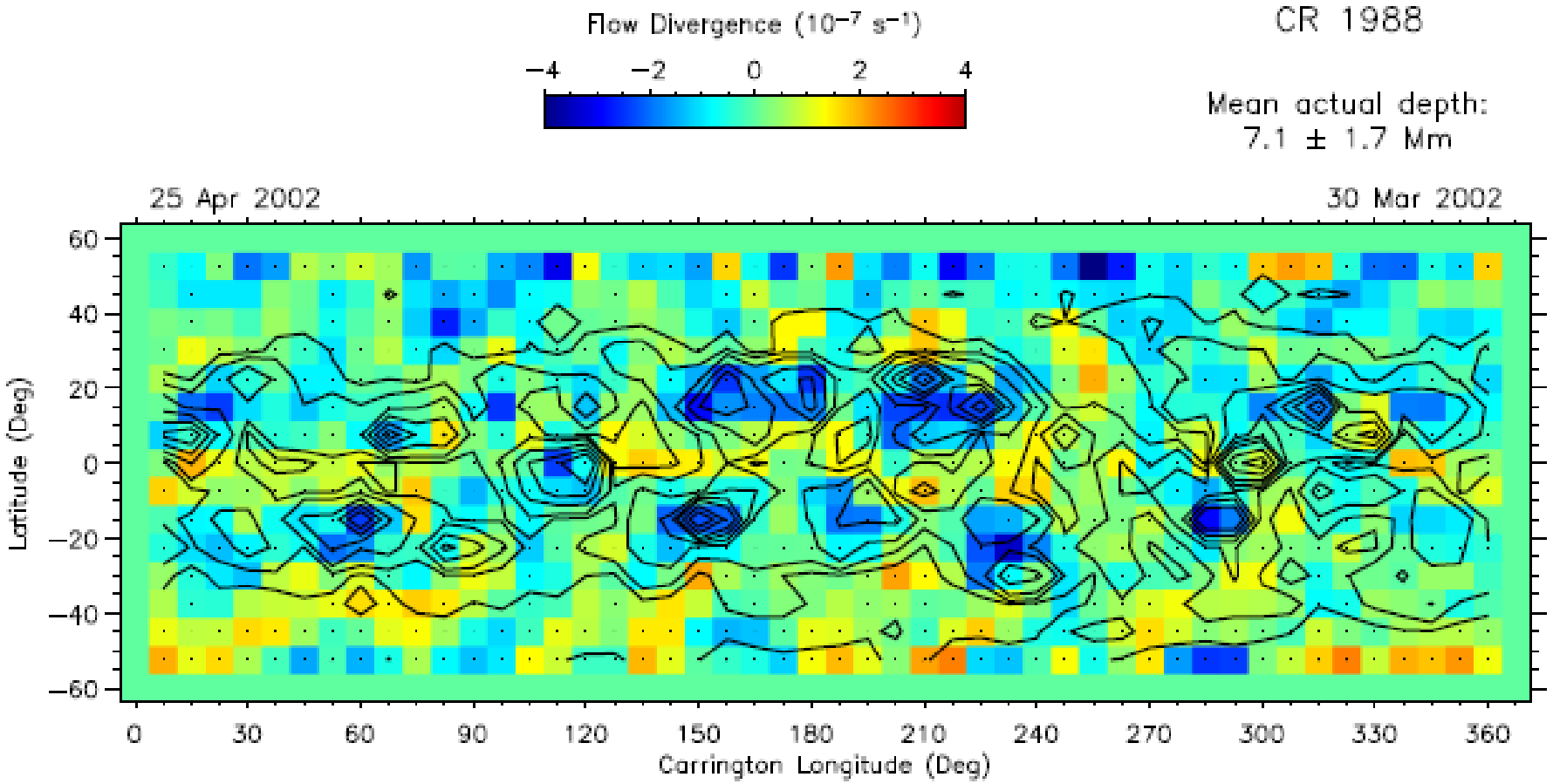

Vertical Velocity (Vz)

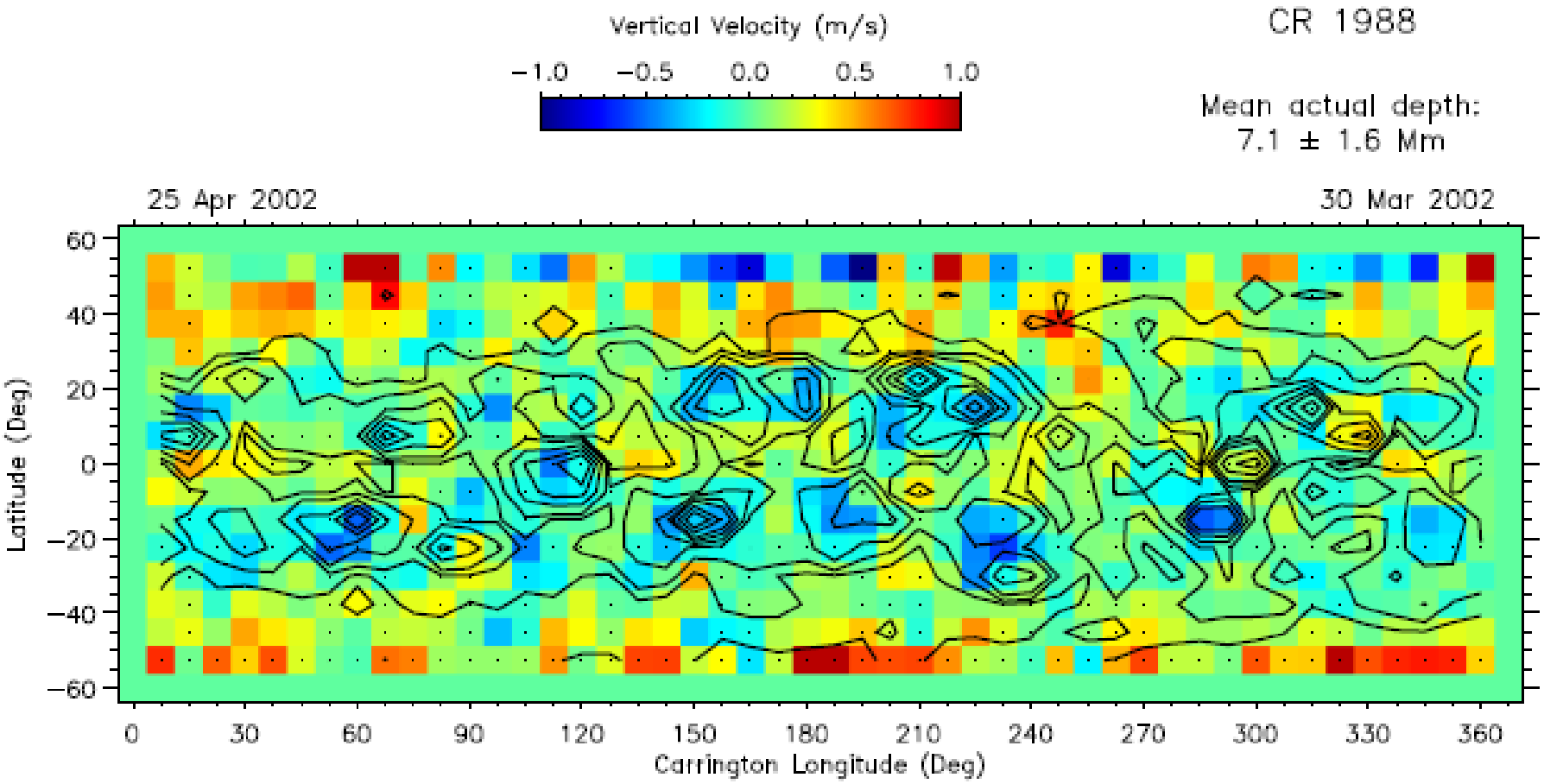

Div v / Vz as a function of depth

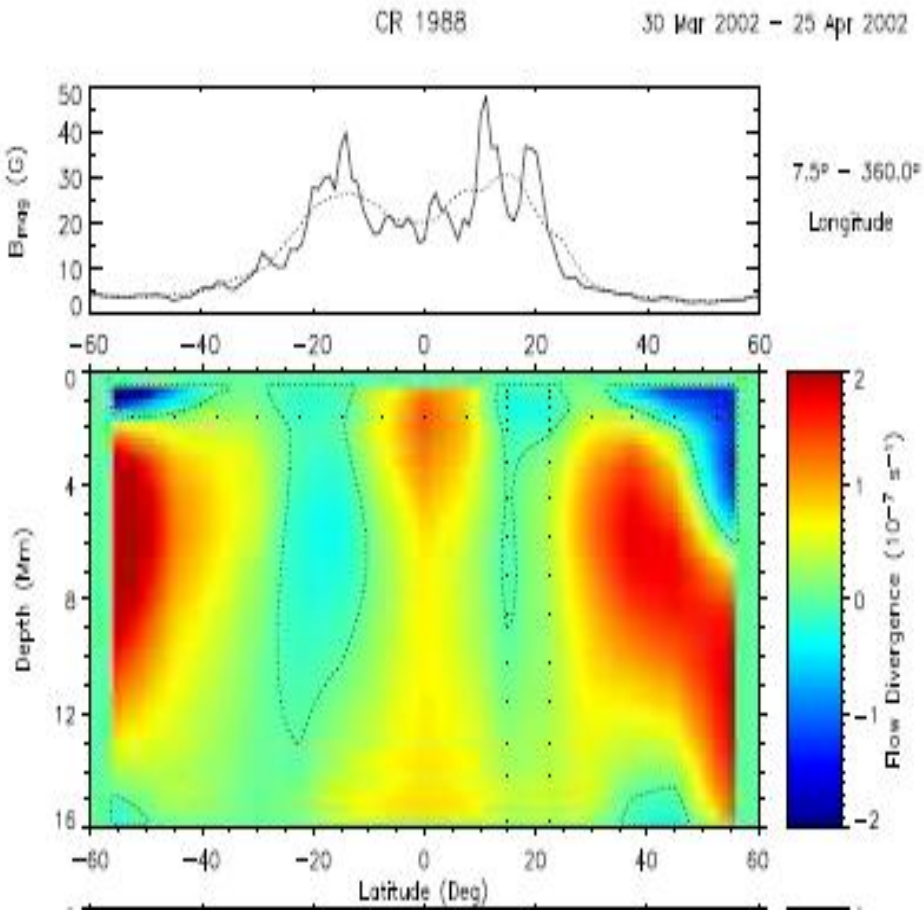

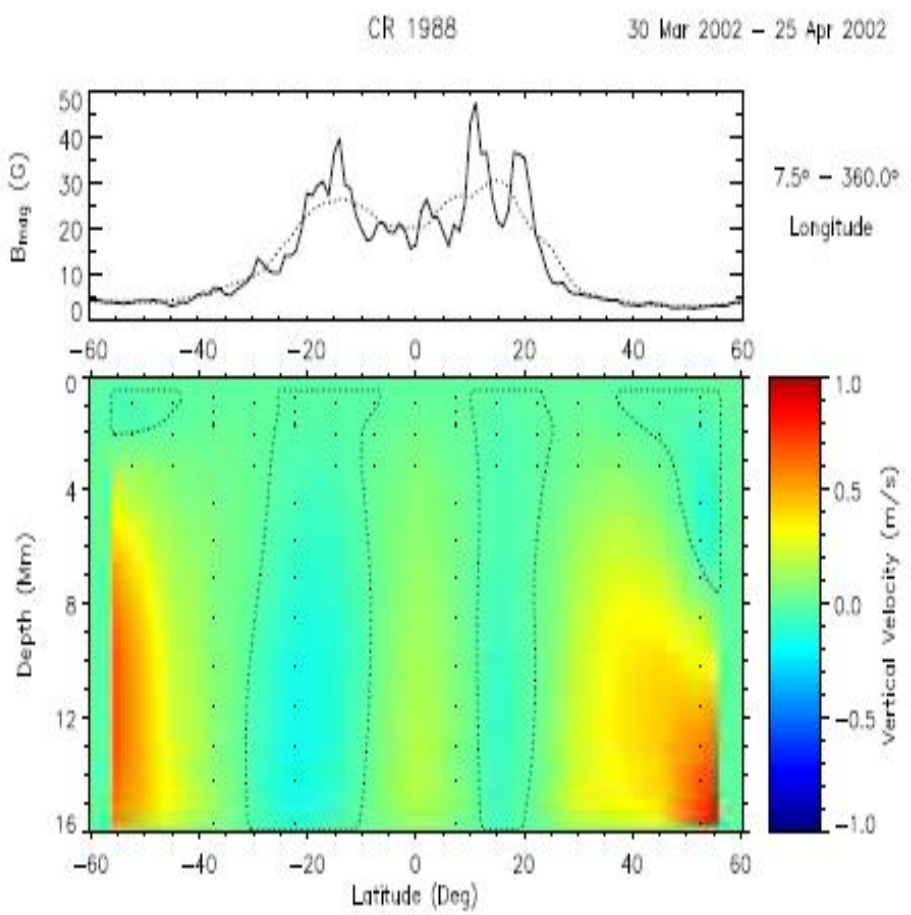

Vertical Velocity as a function of depth for 3 levels of magnetic activity

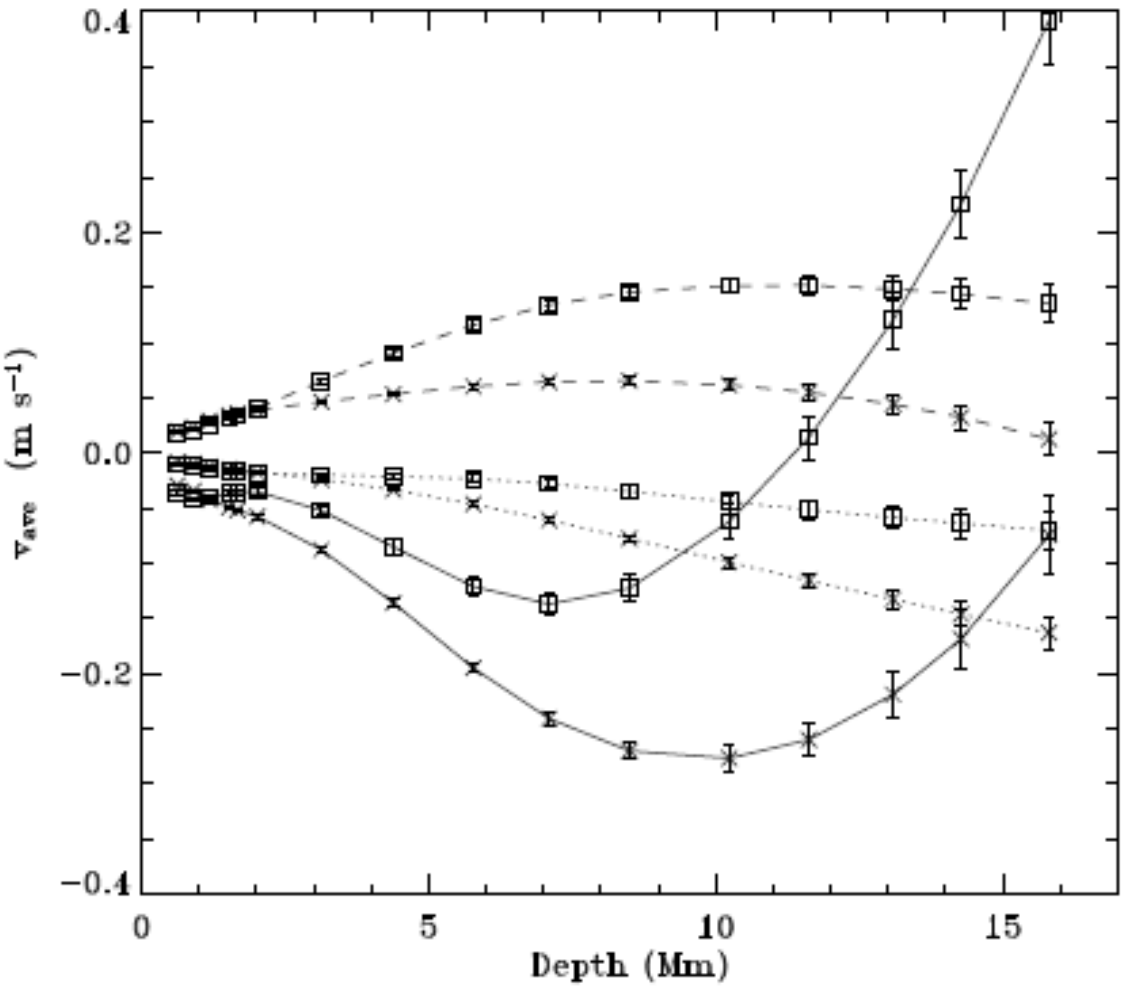

- Low B => up flows
  B< 9G
- Medium B => Down flows
  9G < B < 54G
- High B => Down flows <10Mm

  Up flows >10Mm
  B > 54G

Selection of areas with different magnetic flux levels over 14 Carrington Rotations

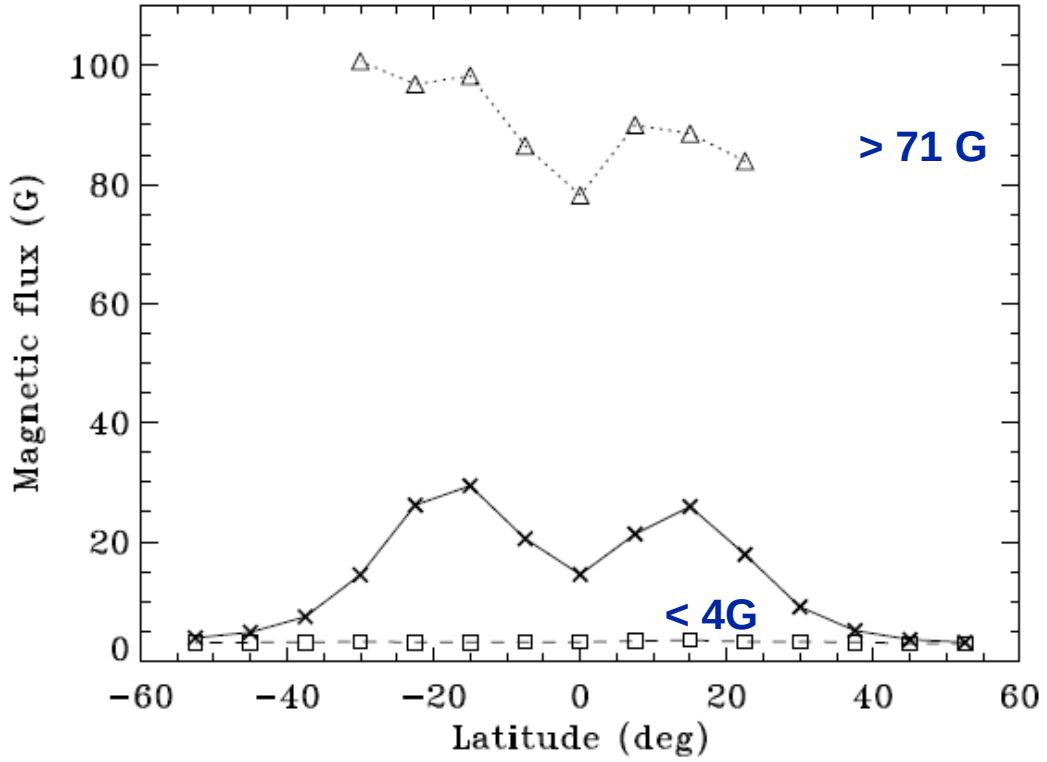

Fig. 1.— The magnetic flux as a function of latitude (solid line, cross symbols) averaged in longitude over CR 1979–1992 (2001, July 27 – 2002, Aug 12). The triangle symbols (dotted line) indicate the average over all locations with magnetic flux greater 71 G and the square symbols (dashed line) indicate the average over 25% of locations with the lowest flux.

V_z averaged over 14 CR

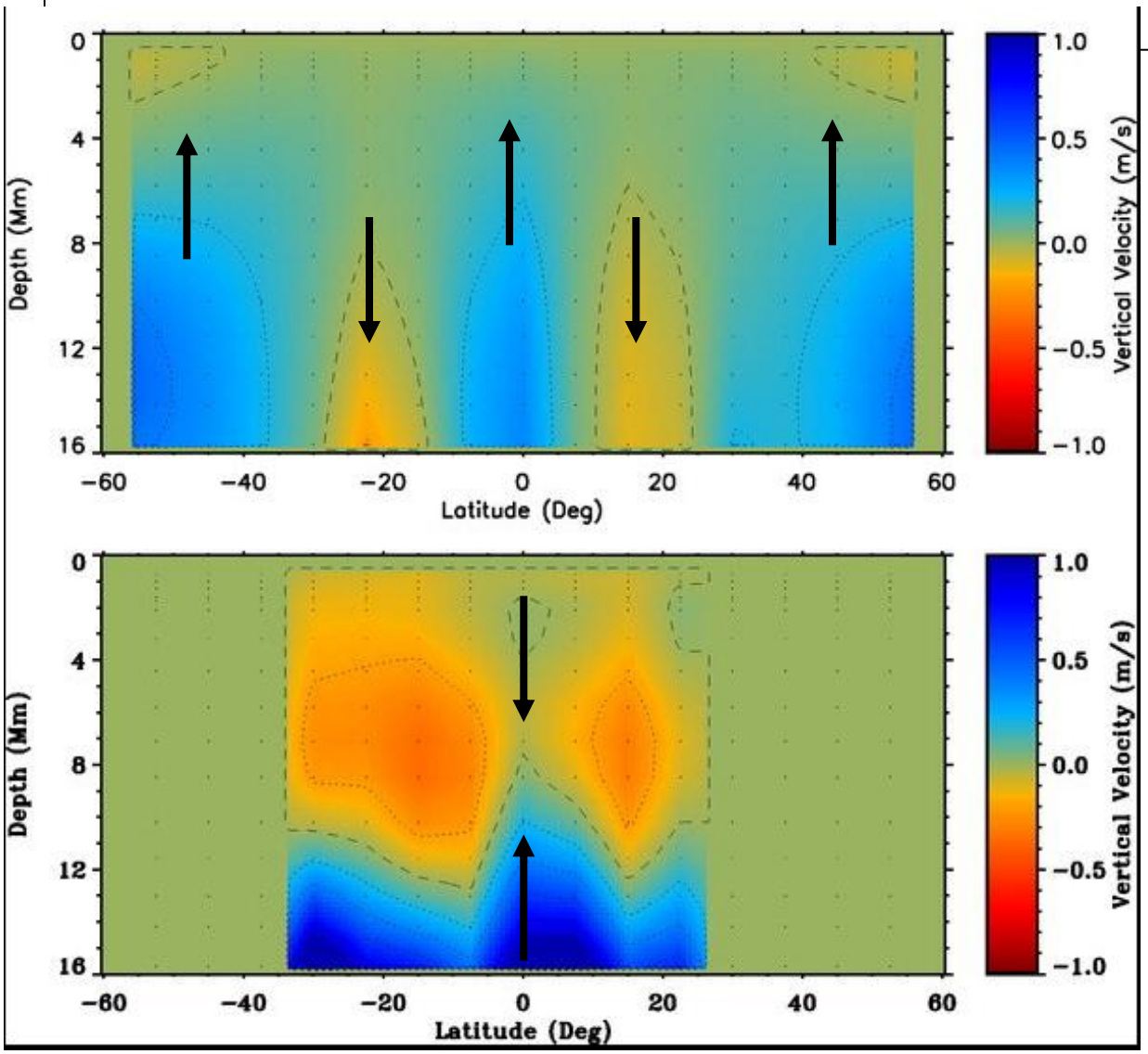

Low activity set

High activity set
B> 71 G

Upflows are typical for flux ropes in convectively unstable layers

Meridional Circulation: Time and depth variation

Polward flow ~10 -20m/s, incresing with depth + secondary flow that converges toward the mean latitude of activity (Haber et al. 2002, Zhao & Kosovichev 2004, Komm et al. 2005)

Counter cells at high latitude (Haber et al. 2002) ?

***González Hernández et al. 2006:* Geometric Calibration issue?**

***Zaatri et al. (2006):* The N/S asymmetry of the flow reflects the N/S assymetry of the magnetic flux.**

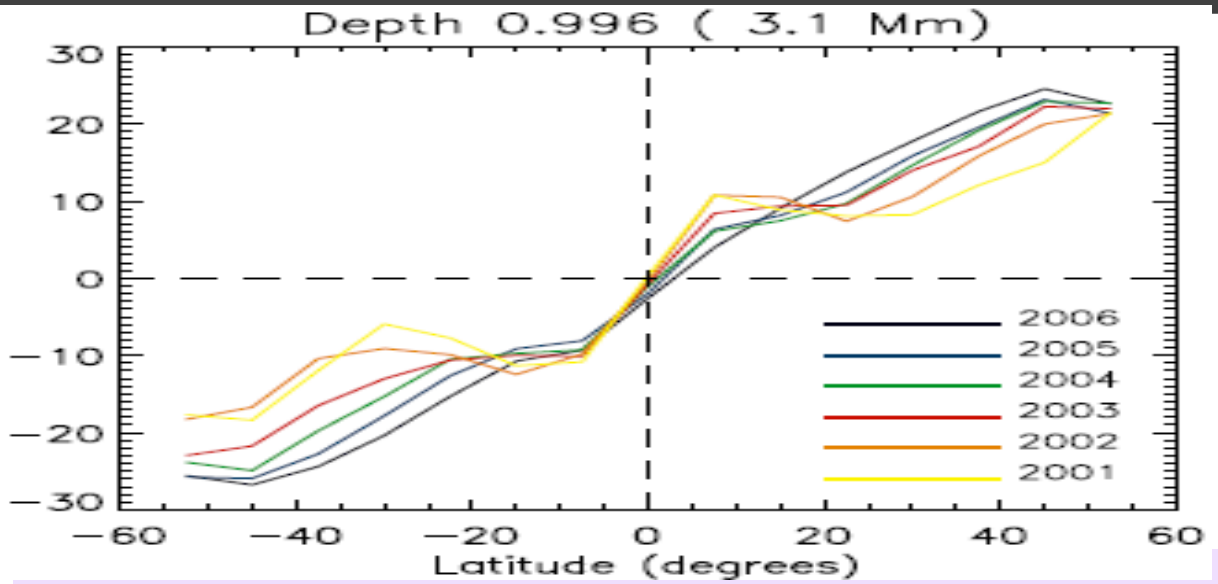

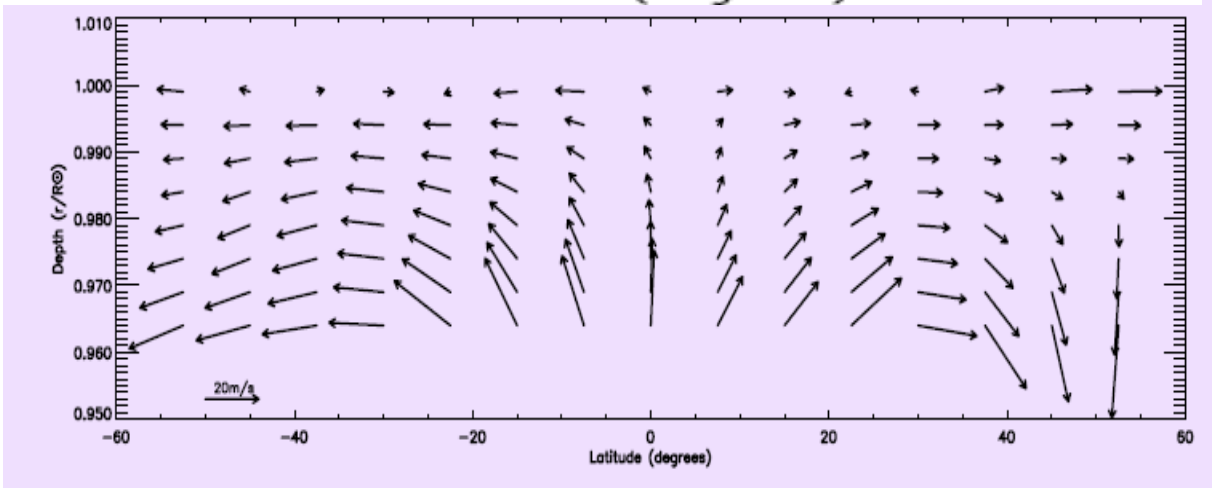

González Hernández et al. 2004, 2008

Residual Meridional Flow V_y averaged over 14 CR

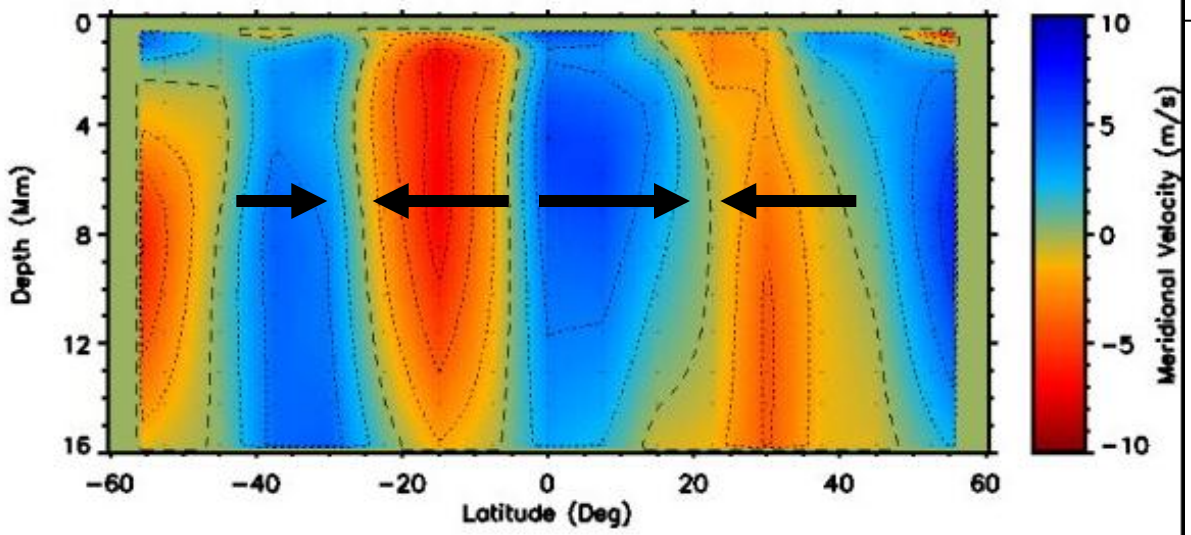

Low activity set

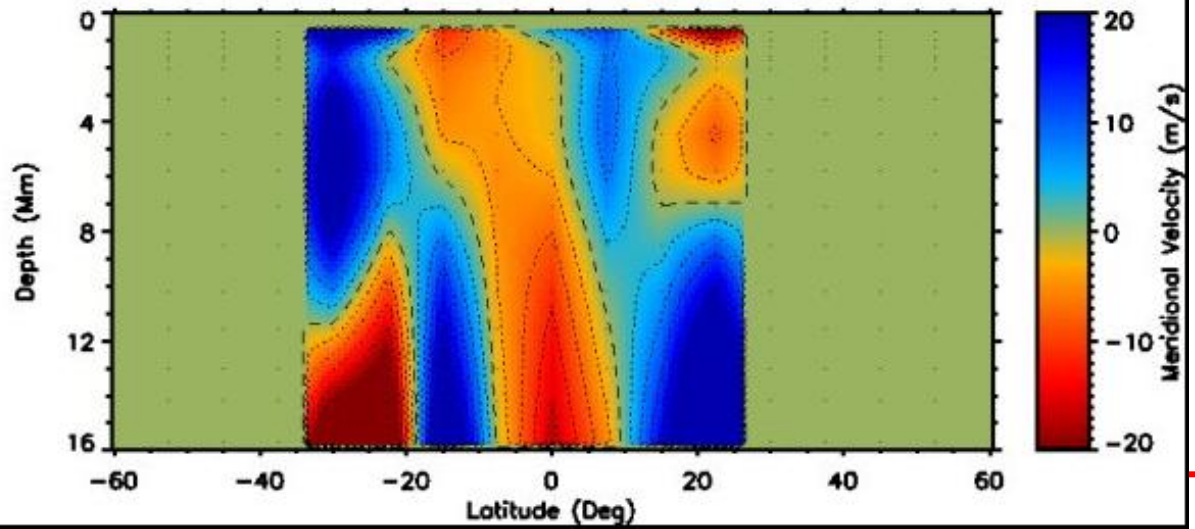

High activity set
B> 71 G

González Hernández et al. 2008

Meridional Circulation: Effect of surface Magnetic Activity?

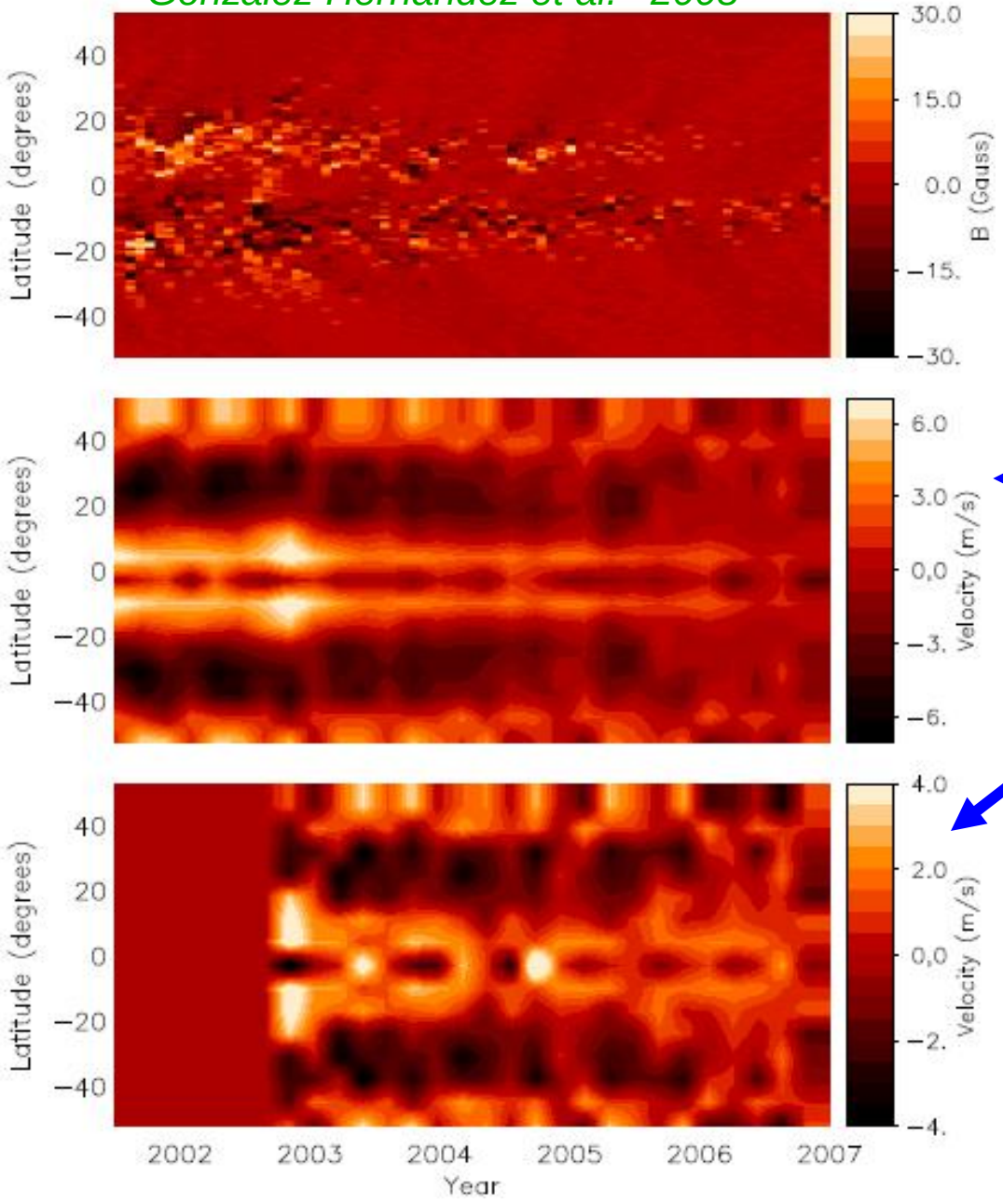

Temporal variation of Meridional circulation Residuals (5.8Mm)

All patches

Quiet Sun only (B<10G at any latitude for a given longitude)

Inflows associated to the activity are confined to the upper layers but persist even after agressively masking surface activity

Synoptic Maps of Kinetic Helicity

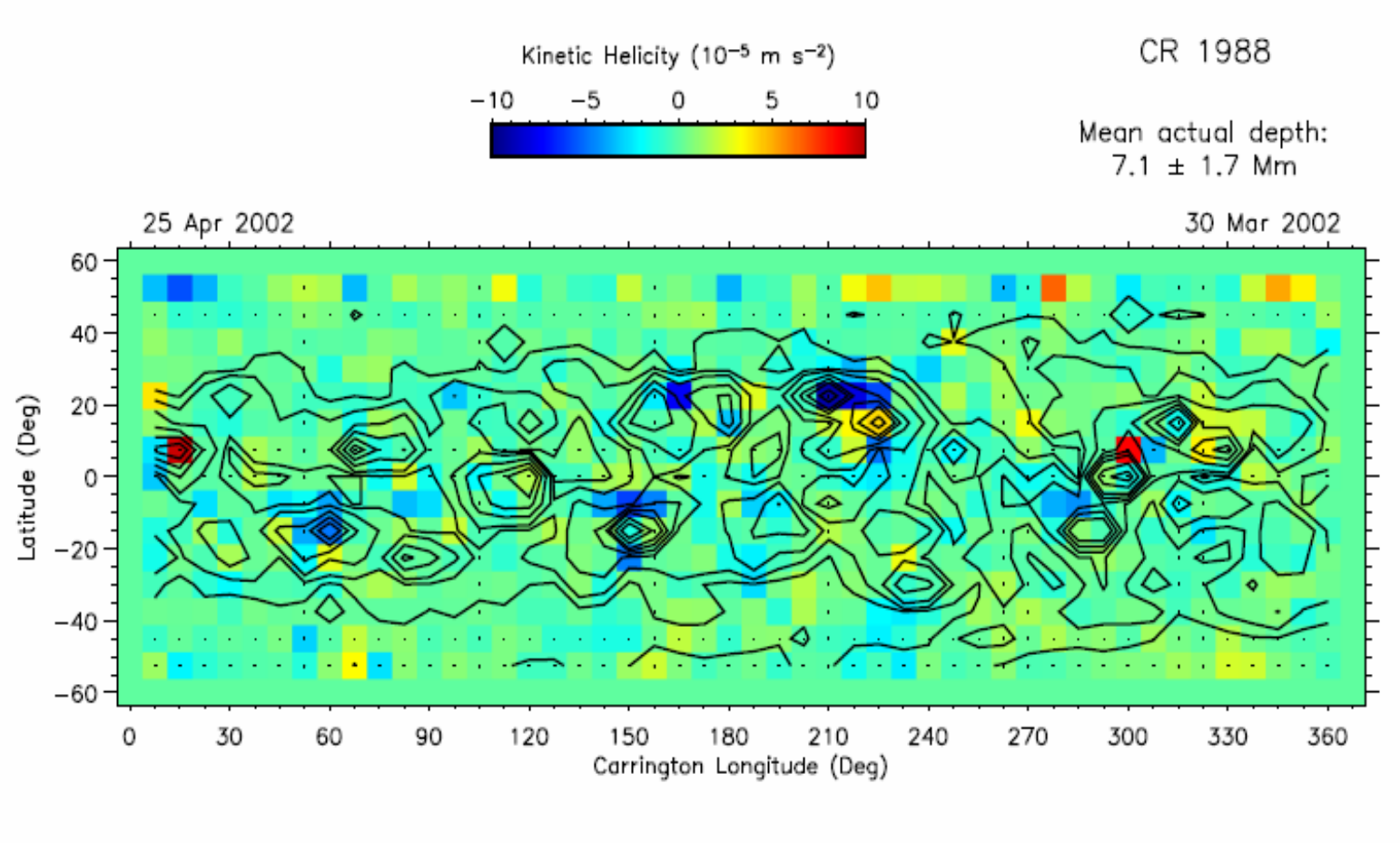

Kinetic Helicity at low activity level

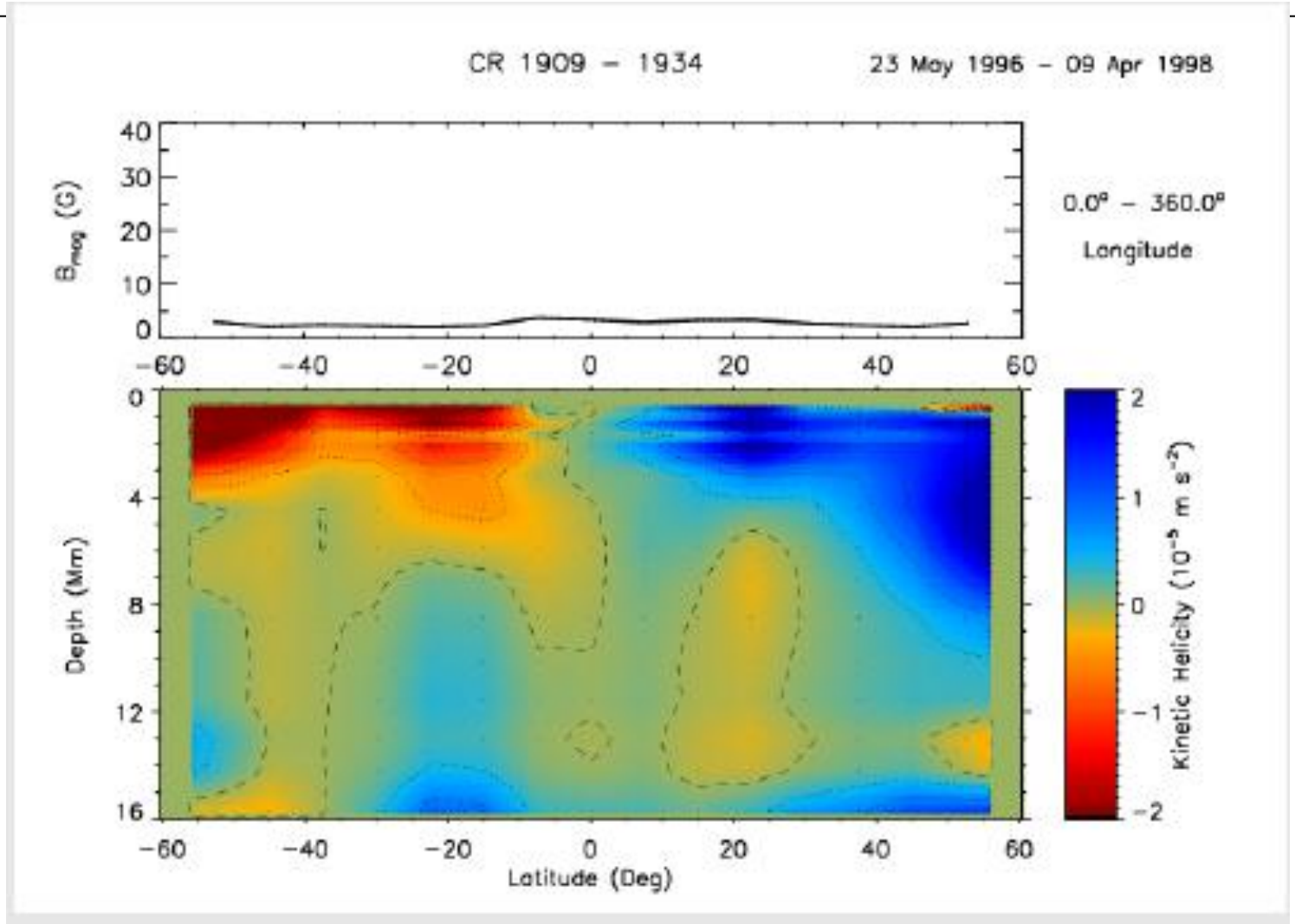

Kinetic Helicity at high activity level

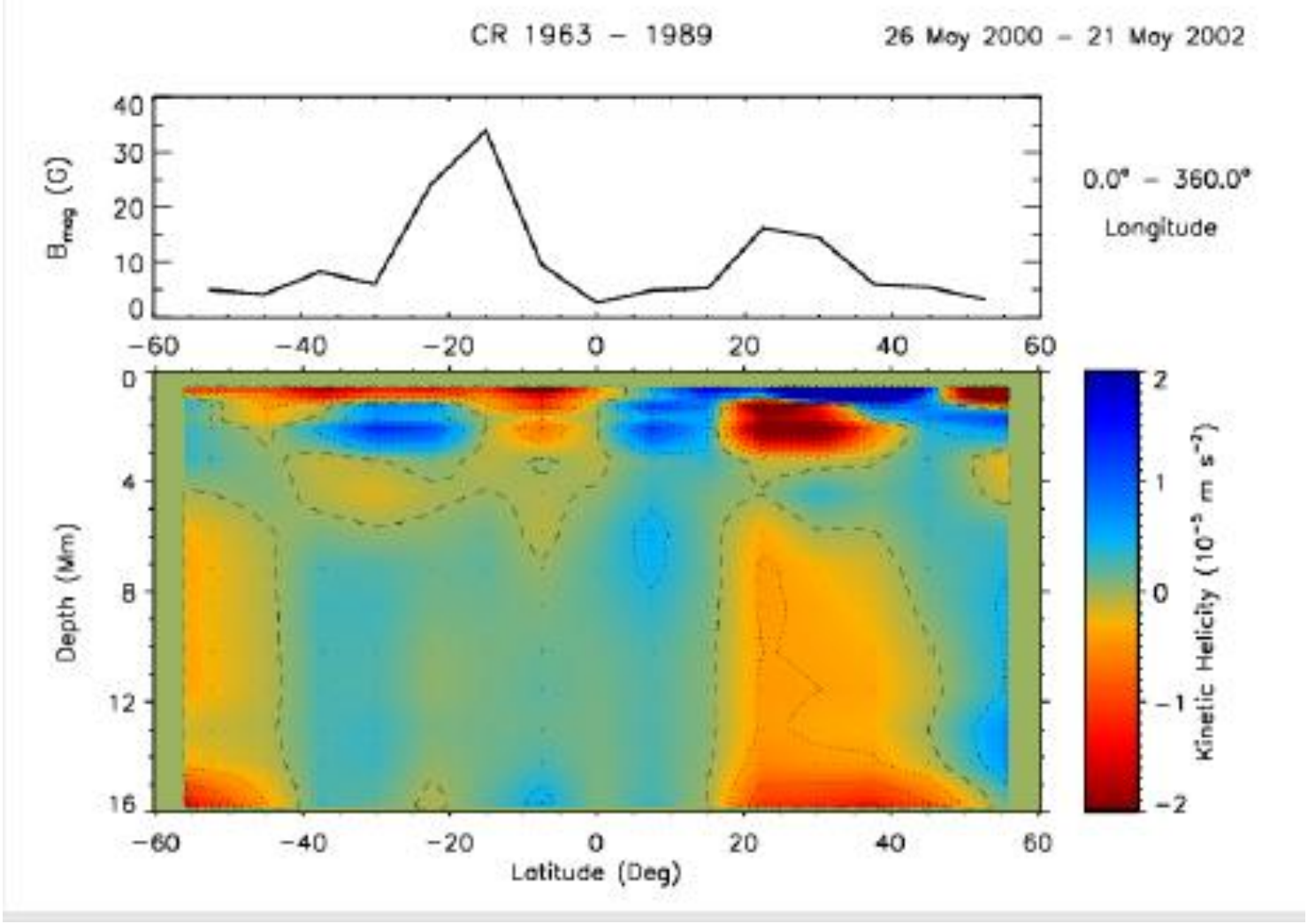

High correlation reported between maximum kinetic helicity density and X-ray Flare intensity *(Komm et al. 2005)*

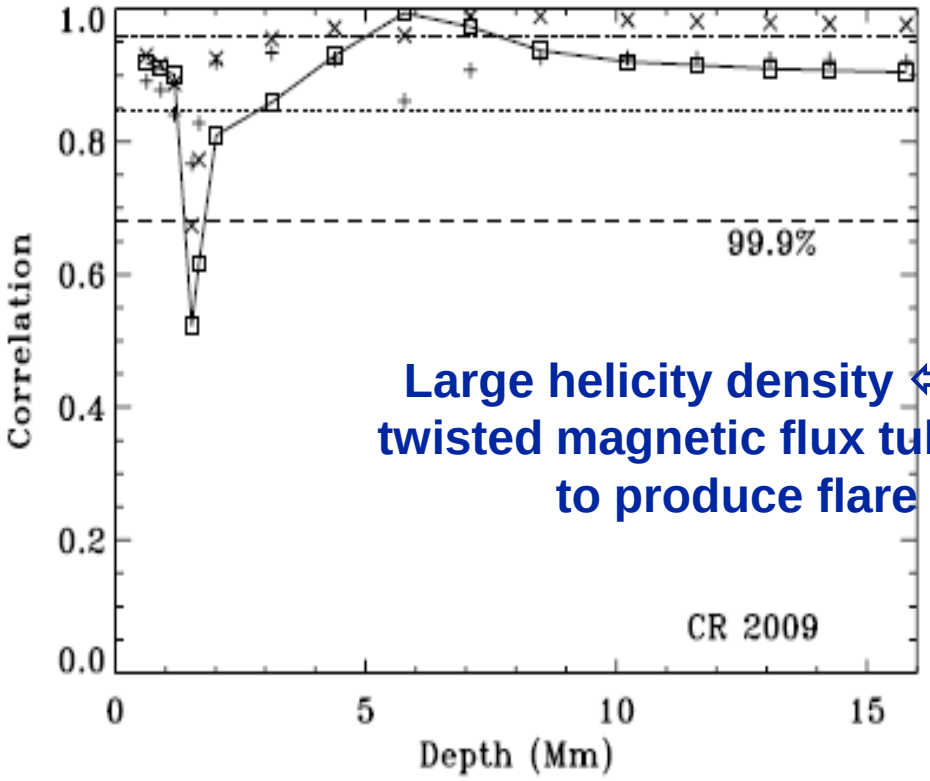

Large helicity density ⇔ highly twisted magnetic flux tubes likely to produce flare ?

FIG. 5.—Linear correlation between maximum kinetic helicity density and X-ray intensity (*squares*), magnetic flux (*plus signs*), and square of magnetic flux (*crosses*) as a function of depth. The correlation between X-ray intensity and magnetic flux (*dotted lines*) and square magnetic flux (*dot-dashed lines*) is included for comparison. The dashed lines indicate the 99.9% confidence level for a given sample size. *Top*: CR 1982, 28 active regions. *Bottom*: CR 2009, 20 active regions.

Does the increase of (unsigned) kinetic helicity coincides with the emergence of flux? (From an analysis of 13 emerging regions)

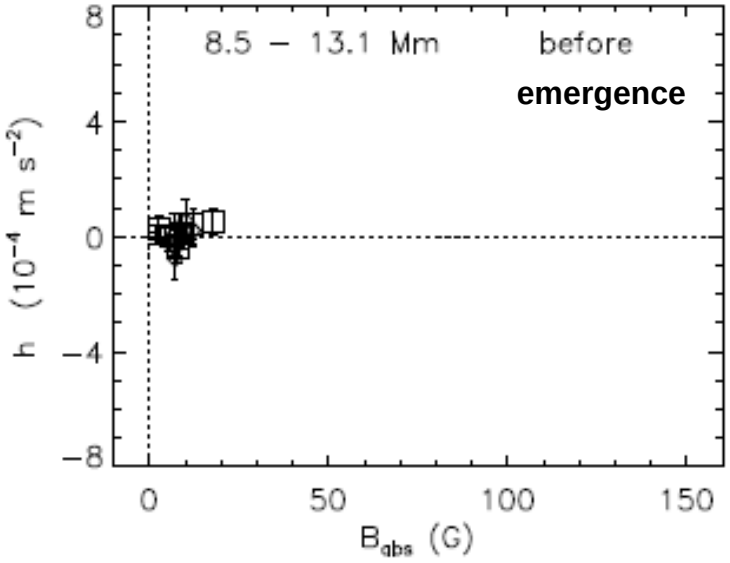

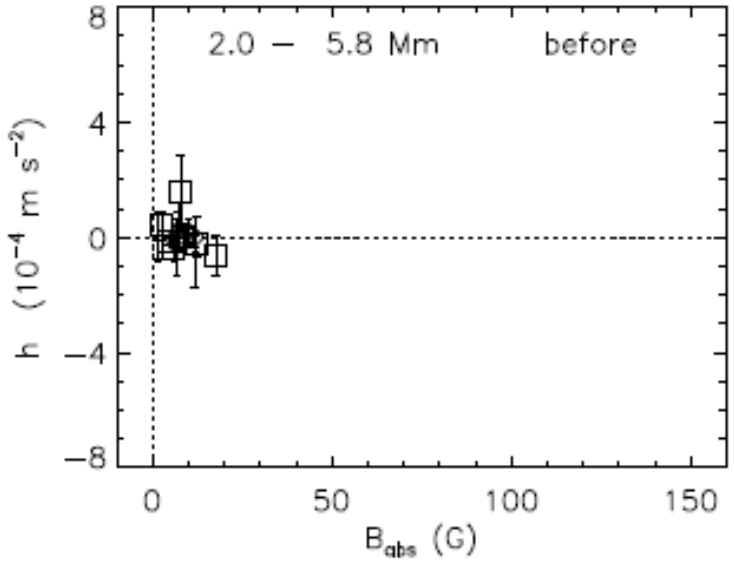

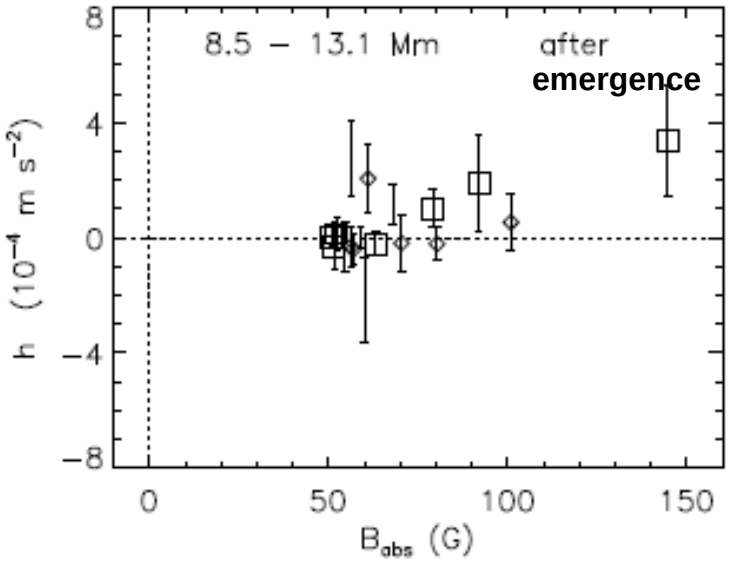

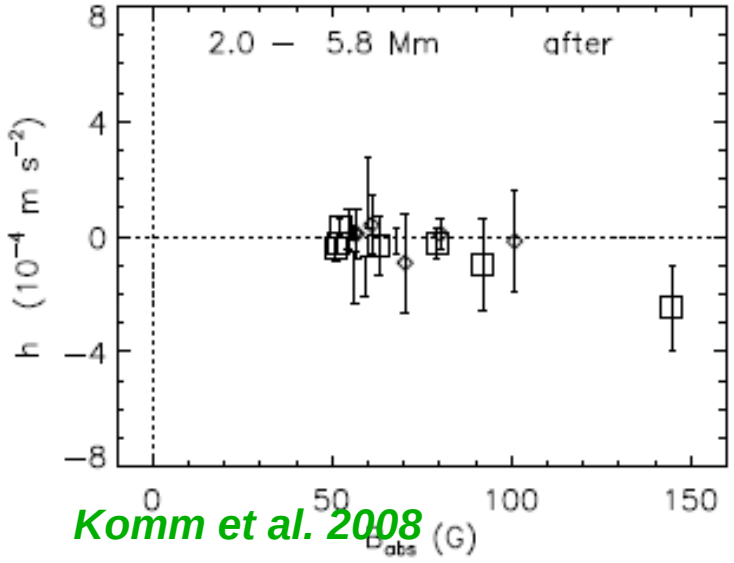

Komm et al. 2008

Does the increase of (unsigned) kinetic helicity coincides with the emergence of flux ?

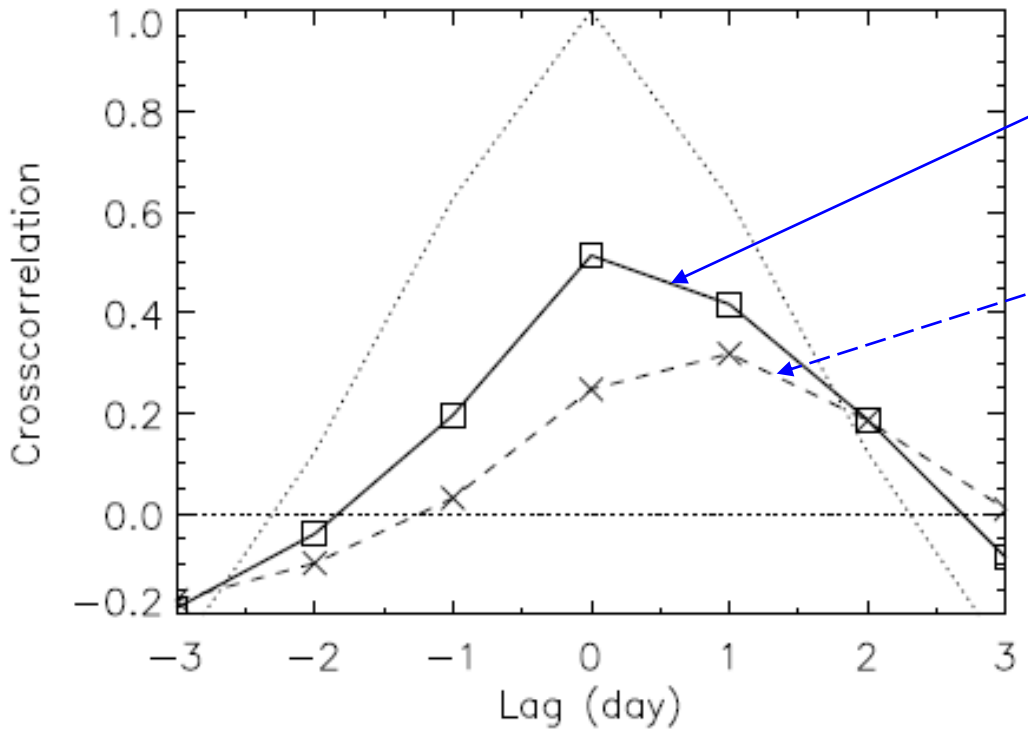

=> The kinetic helicity in shallow layers lags behind the kinetic helicity in deeper layers.

Also: there is a preference for upflows before the emergence of new flux and for a transition towards downflows after flux emergence

Komm et al. 2008

Direct sensing of B with ring analysis ?

Dispersion relation: *(Kosovichev et al. 1997)*

$$(\omega - \vec{k}.\vec{v})^2 = \omega_{ac}^2 + \frac{k^2}{2}\left(c^2 + c_A^2 + \sqrt{(c^2 + c_A^2)^2 - 4c^2(\vec{k}.\vec{c}_A)^2 / k^2} \right)$$

3D velocity field

Acoustic cut off frequency

Alvén velocity

$$\vec{c}_A = \frac{\vec{B}}{\sqrt{4\pi\rho}}$$

- Temperature perturbations => do not depend on the direction of propagation
- Flow perturbations => waves move faster along the flow
- Magnetic fields perturbations => waves traveling perpendicular to the field lines are the most sensitive to B (wave speed anisotropy not yet detected)

Ryutova & Scherrer 1998

$$P(k_x, k_y, \omega) = A/\left((\Gamma/2)^2 + [\omega - \omega_0 - (v_x k_x + v_y k_y) - (\delta\omega_0 + \delta\omega_c \cos 2\theta + \delta\omega_s \sin 2\theta)]^2\right)$$

$$\delta\omega_o = \frac{k_h^2}{2\pi\omega_o} \int_0^{z_t} \frac{v_A^2 dz}{\sqrt{z(z_t - z)}} \left(\frac{z_t}{z} - \frac{1}{2}\right) \qquad (5a)$$

$$\delta\omega_c = \frac{k_h^2}{2\pi\omega_o} \int_0^{z_t} \frac{dz}{2\sqrt{z(z_t - z)}} \left(v_{Ay}^2 - v_{Ax}^2\right) \qquad (5b)$$

$$\delta\omega_s = -\frac{k_h^2}{2\pi\omega_o} \int_0^{z_t} \frac{dz}{\sqrt{z(z_t - z)}} v_{Ax} v_{Ay}. \qquad (5c)$$

Hill, Haber & Zweibel (1996)

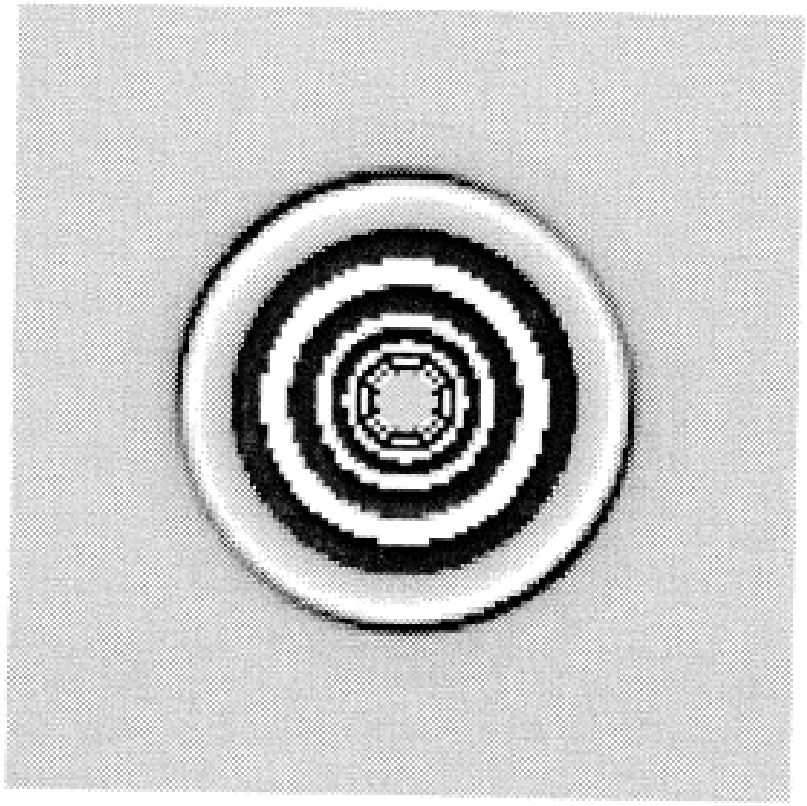

Figure 1: The difference between simulated ring diagrams with and without an underlying magnetic field. The change in shape of the rings can be clearly seen as a change in contrast in the outermost ring. Also visible is the change in the radii of the inner rings.

Hill, Haber & Zweibel (1996)

Many other effects can influence the ring shape profile:

- **Flow inhomogeneity within a patch**
- **Damping**
- **Excitation**
- **Scattering of acoustic waves**
- **Spatially localized wave emission**
- **Noise correlated with oscillation signal**
- **…..**

Conclusions

- Rings are sensitive to Activity (to local and(?) global field)
  - Sensitivity to local field can be seen as a source of noise when one try to infer global flows (meridional, zonal) and how they vary with the cycle (torsional) => filtering , how and to what level ?
  - Pattern of global flows independent of activity level but their magnitude vary.
  - When patches are sorted as a function of some MAI, it gives some hints on how the flow are organized below and around active regions.
  - Lots of efforts are now made in trying to detect correlations between activity events (CMEs, flares, filaments…) and some descriptors of the submerge flows (helicity) or underlying waves (linewidth) essentially in the hope of finding precursor indicators

Conclusions

- A lot of efforts have been made during the last few years but should be continued in:
  - Making comparison between the different Methods (group LoHCO)
  - Understanding errors, methods resolution and correlations
  - Understanding effects of image misalignment / geometric effects (P-angle / Bo angle)
- New developments
  - High resolution Ring Analysis using f-modes *(B. Hindman, D. Haber et al.)*
  - Deeply penetrating Ring techniques *(I. Gonzalez-Hernandez et al.)*
  - 3D Kernels and inversion procedure
  - Structural inversion of ring frequency shifts (Basu et al.)
  - Simultaneous use of intensity and velocity signals (SDO, PICARD…)